KA–TP–14–2000
hep-ph/0008308

The MSSM prediction for $W^{\pm}H^{\mp}$ production by gluon fusion at the Large Hadron Collider

Oliver Brein [1], **Wolfgang Hollik** [2], **Shinya Kanemura** [3]

Institut für Theoretische Physik, Universität Karlsruhe,
D-76128 Karlsruhe, Germany

Abstract

We discuss the associated $W^{\pm}H^{\mp}$ production in pp collision for the Large Hadron Collider. A complete one-loop calculation of the loop-induced subprocess $gg \to W^{\pm}H^{\mp}$ is presented in the framework of the Minimal Supersymmetric Standard Model (MSSM), and the possible enhancement of the hadronic cross section is investigated under the constraint from the squark direct-search results and the low-energy precision data. Because of the large destructive interplay in the quark-loop contributions between triangle-type and box-type diagrams, the squark-loop contributions turn out to be comparable with the quark-loop ones. In particular, the hadronic cross section via gluon fusion can be extensively enhanced by squark-pair threshold effects in the box-type diagrams, so that it can reach the size of the hadronic cross section via the subprocess $b\overline{b} \to W^{\pm}H^{\mp}$ which appears at tree level.

[1]E-mail: obr@itp.uni-karlsruhe.de
[2]E-mail: Wolfgang.Hollik@physik.uni-karlsruhe.de
[3]E-mail: kanemu@itp.uni-karlsruhe.de

1 Introduction

In the Standard Model (SM), a single neutral Higgs boson is predicted as a direct consequence of the SM mechanism of electroweak symmetry breaking. The detection of this particle is, therefore, one of the most essential tasks at present and future collider experiments, especially at the Large Hadron Collider (LHC) [1]. On the other hand, charged Higgs bosons (as well as a CP-odd neutral Higgs boson) are predicted in extended versions of the SM model, including the Minimal Supersymmetric Standard Model (MSSM). Since a discovery of such an additional Higgs boson will immediately indicate physics beyond the SM, there is increasing interest in theoretical and experimental studies to provide the basis for its accurate exploration.

At hadron colliders, a mode for the charged Higgs boson $H^\pm$ detection may be the top-antitop pair production from gluon fusion and $q\bar{q}$ annihilation and subsequent decay $t \to bH^+ \to b\tau^+\nu$, if the mass of $H^\pm$ is smaller than $m_t - m_b$. For heavier $H^\pm$, main modes for the $H^\pm$ production may be those associated with heavy quarks, such as $gb \to H^-t$ [2] and $qb \to q'bH^-$ [3]. Although these processes give rather large production rates, they suffer from also large QCD backgrounds, especially when the $H^\pm$ mass is above the threshold of $t\bar{b}$ pair production. Pair production of $H^\pm$ via the tree-level $q\overline{q}$ annihilation subprocesses and via the loop-induced gluon-fusion mechanism have also been studied in the literature [4, 5, 6, 7].

A further possibility is single charged-Higgs-boson production together with a charged W gauge boson. In this paper we focus on the discussion of this process of associate $W^\pm H^\mp$ production for the LHC. There are mainly two partonic subprocesses that contribute to the hadronic cross section $pp \to W^-H^+$: the $b\bar{b}$ annihilation (at the tree level) and the gg fusion (at the one-loop level). The production cross section based on $gg \to W^\pm H^\mp$ can be comparable to that via $b\overline{b} \to W^\pm H^\mp$, because of the large number of gluons in the high energy proton beams at the LHC. The associate $W^\pm H^\mp$ production via $b\overline{b}$ annihilation and the gg fusion have been discussed at first in [8] for a supersymmetric 2-Higgs-doublet model including the loop contributions from top and bottom quarks with the approximation $m_b = 0$. That work has been extended in [9] including a non-zero b-quark mass, thus allowing the investigation of the process for arbitrary values of $\tan\beta$. The rate of $W^\pm H^\mp$ production mediated by the quark loops turned out to be sizable, especially for low and high values of $\tan\beta$. The background, which mainly comes from $t\overline{t}$ production, has been analysed in [10]. These studies correspond to a MSSM scenario where the scalar quarks are sufficiently heavy to decouple from the loop contributions.

In more general scenarios the squarks need not be heavy, and taking the MSSM seriously requires the inclusion of also the squark loops in the gluon-fusion mechanism and to study their effects on the predictions for $pp \to W^-H^+$. There are several reasons to

underline the importance of the squark contributions. In the subprocess $gg \to W^\pm H^\mp$, the quark-loop contributions are destructive between the triangle-type diagrams and the box graphs [8, 9] in the MSSM; the effects from both types are almost of the same size, so that the cross section obtained from the summed t-b loop contributions is more than one order of magnitude smaller than that with only triangle- or box-type diagrams separately. By this mechanism of cancellation in the quark-loop terms the relative importance of the squark-loop contribution increases. On top, the cross section for $gg \to W^\pm H^\mp$ can be sizeably enhanced by threshold effects of squark pairs, such that in special cases the hadronic cross section via gluon fusion can be as large as that via $b\bar{b} \to W^\pm H^\mp$. Moreover, the present calculation of the $b\bar{b}$ annihilation is expected to overestimate the cross section, as it has been mentioned [8, 9] by recalling the problem of double counting[11]. Owing to the presence of also the superpartners in the virtual states of the loop diagrams, the gluon-fusion mechanism is more sensitive to the detailed structure of the model than the tree-level process of $b\bar{b}$ annihilation.[4]

In this article we extend the previous calculations by including also the scalar-quark sector in the loop diagrams for gg fusion. We give analytical results and a detailed discussion of the effects in the hadronic cross section. Our results are for general parameters of the MSSM; for the numerical discussion, constraints from the direct search and from the precision data [13, 14] are taken into account.[5]

The paper is organized as follows. In Section 2 the calculation for the partonic cross section, $gg \to W^- H^+$, is explained, and numerical results for the partonic and hadronic cross sections are presented in Section 3. Our conclusion is given in Section 4. All the relevant coupling constants and the analytic formulae for the amplitudes are presented in the Appendix for a comprehensive documentation.

2 The partonic process $gg \to W^- H^+$

2.1 Cross section

In our kinematical conventions, the momenta of the initial state gluons, k and $\bar{k}$, are chosen as incoming and outgoing for the momenta, p and $\bar{p}$, of the final state particles:

$$g(k, a, \sigma) + g(\overline{k}, b, \overline{\sigma}) \to W^-(p, \lambda) + H^+(\overline{p})\,.$$

[4] For the subprocess $b\bar{b} \to W^- H^+$, the electroweak one-loop corrections have recently been studied in Ref. [12], which can give rise to a 10-15% reduction of the lowest-order result.

[5] Quite recently, the squark-loop contributions to gluon fusion have also been derived [15] with a study of their effects in a supergravity-inspired GUT scenario.

Besides by their momenta, the initial state gluons are characterized by their color indices a, b and their helicities $\sigma, \bar{\sigma}$ $(= \pm 1)$, and the final state W boson is characterized by its helicity λ $(= 0, \pm 1)$. We make use of the parton kinematical invariants

$$\hat{s} = (k + \overline{k})^2 \,, \quad \hat{t} = (k - p)^2 \,, \quad \hat{u} = (k - \overline{p})^2$$

obeying the relation

$$\hat{s} + \hat{t} + \hat{u} = m_{H^\pm}^2 + m_W^2 \quad .$$

The spin- and color-averaged cross section for the parton process

$$\frac{d\sigma}{d\hat{t}} = \frac{1}{16\pi \hat{s}^2} \sum_{\lambda=0,\pm} \frac{1}{4} \sum_{\sigma,\bar{\sigma}=\pm 1} \frac{(\mathrm{CF})}{64} \left| \mathcal{M}_{\sigma\bar{\sigma}\lambda} \right|^2, \;\; \text{with} \;\; (\mathrm{CF}) = \sum_{a,b=1}^{8} \left[\mathrm{Tr}\{ \frac{\lambda^a}{2} \frac{\lambda^b}{2} \} \right]^2 = 2, \tag{1}$$

contains the helicity amplitudes

$$\mathcal{M}_{\sigma\bar{\sigma}\lambda} = \varepsilon_\sigma^\mu(k) \varepsilon_{\bar{\sigma}}^\nu(\overline{k}) \varepsilon_\lambda^{*\rho}(p) \, \widetilde{\mathcal{M}}_{\mu\nu\rho} \quad , \tag{2}$$

where $\varepsilon_\sigma^\mu(k)$, $\varepsilon_{\bar{\sigma}}^\nu(\overline{k})$ and $\varepsilon_\lambda^{*\rho}(p)$ are the polarization vectors for incoming gluons and outgoing W bosons. As a general feature of the amplitude, the transversality of gluons gives useful identities

$$k^\mu \varepsilon_{\bar{\sigma}}^\nu(\overline{k}) \varepsilon_\lambda^{*\rho}(p) \, \widetilde{\mathcal{M}}_{\mu\nu\rho} = \varepsilon_\sigma^\mu(k) \overline{k}^\nu \varepsilon_\lambda^{*\rho}(p) \, \widetilde{\mathcal{M}}_{\mu\nu\rho} = 0 \quad , \tag{3}$$

which allow cross-checks of our one-loop calculation of $\widetilde{\mathcal{M}}_{\mu\nu\rho}$.

In the parton Center-of-Mass (CM) frame, the momenta may be expressed by

$$k^\mu = \left(\frac{\sqrt{\hat{s}}}{2}, 0, 0, \frac{\sqrt{\hat{s}}}{2} \right), \tag{4}$$

$$\overline{k}^\mu = \left(\frac{\sqrt{\hat{s}}}{2}, 0, 0, -\frac{\sqrt{\hat{s}}}{2} \right), \tag{5}$$

$$p^\mu = (E_W, \vec{p}_W) = (E_W, |\vec{p}_W| \sin\Theta, 0, |\vec{p}_W| \cos\Theta) \,, \tag{6}$$

and then the polarization vectors are given by

$$\varepsilon_\sigma^\mu(k) = \frac{1}{\sqrt{2}} (0, 1, i\sigma, 0) \,, \tag{7}$$

$$\varepsilon_{\bar{\sigma}}^\mu(\overline{k}) = \frac{1}{\sqrt{2}} (0, 1, -i\overline{\sigma}, 0) \,, \tag{8}$$

and

$$\varepsilon_{\lambda=0}^{*\mu}(p) = \left(\frac{|\vec{p}_W|}{m_W}, \frac{E_W}{m_W} \sin\Theta, 0, \frac{E_W}{m_W} \cos\Theta \right), \tag{9}$$

$$\varepsilon_{\lambda=\pm}^{*\mu}(p) = \frac{1}{\sqrt{2}} (0, i\lambda \cos\Theta, 1, -i\lambda \sin\Theta) \,. \tag{10}$$

Finally, the integrated partonic cross section

$$\sigma_{gg\to W^-H^+}(\hat{s}, \alpha_S(\mu_R)) = \int_{\hat{t}_{\min}(\hat{s})}^{\hat{t}_{\max}(\hat{s})} d\hat{t}\, \frac{d\sigma}{d\hat{t}} \tag{11}$$

is evaluated by numerical integration over the kinematically allowed $\hat{t}$-range for a given CM-energy $\sqrt{\hat{s}}$. The renormalization scale μ_R in the $\overline{\rm MS}$ strong coupling constant $\alpha_S(\mu)$ is chosen as $\sqrt{\hat{s}}$, the hard energy scale of the process.

2.2 Calculation of the amplitude

In the MSSM, there is no tree-level contribution to the subprocess $gg \to W^-H^+$. The process is induced at the one-loop level by diagrams with quark-loops (see Appendix D.1) and with squark-loops (see Appendix D.2). In the loop diagrams, also the neutral Higgs bosons h^0, H^0 and A^0 of the MSSM appear as well as the scalar partners of the quarks. Notations and couplings are collected in Appendix C.

The quark-loop diagrams can be subdivided into box-type diagrams and into triangle diagrams with s-channel exchange of a neutral Higgs boson. In each box diagram, the quarks in the loop couple directly to the outgoing charged Higgs boson H^+, while in the triangle diagrams the quarks couple to one of the neutral Higgs bosons h^0, H^0 and A^0. Since these Yukawa interactions are all proportional to the quark masses, the contributions from the loop diagrams of the third-generation quarks (t, b) are dominant.

It has been known that there is a striking feature among the quark-loop contributions to the amplitude in the MSSM. Owing to supersymmetry, the box-diagram contribution to the amplitude and the triangle-type one are almost of the same size but the relative sign is negative, so that strong destructive interference occurs. The cross section resulting from all the quark-loop diagrams is therefore one to two orders of magnitude smaller than the cross section obtained from only box-type diagrams or only triangle diagrams, separately.

By the destructive interference in the quark-loop contributions, the squark-loop effects become relatively large. The squark one-loop diagrams are subdivided into (1) diagrams with a 2-point loop and an intermediate s-channel neutral CP-even Higgs boson, (2) diagrams with a triangle and an intermediate neutral CP-even Higgs boson, (3) diagrams with a triangle without an intermediate Higgs boson, and (4) box-type diagrams. As has been verified explicitly, each group separately fulfills the transversality relations (3).

The cross section has been derived in two completely independent calculations and perfect agreement has been achieved. Furthermore, these results have been confirmed by utilizing FeynArts and FormCalc [16]. The agreement of these three independent calculations and the transversality test establish strong confidence in our result.

3 Numerical Results

3.1 Parameters

We take m_Z, m_W and G_F as the input electroweak parameters, and use values $m_Z = 91.1882$ GeV, $m_W = 80.419$ GeV and $G_F = 1.16639 \times 10^{-5}$ GeV^{-2} [13]. For the strong coupling constant $\alpha_S(\mu_R)$, we use the formula including the two-loop QCD corrections for $n_f = 5$ with $\Lambda^5_{QCD} = 170$ MeV which can be found in [13]. The mass of the top and bottom quarks are fixed here as $m_t = 174.3$ GeV and $m_b = 4.7$ GeV.

The sfermion parameter sets are chosen in accordance with the direct search results [13]. In addition, the stringent experimental constraints on the new physics parameters from the electroweak precision measurements are respected. In Refs. [14, 17], this kind of constraint on the new physics parameters has been studied in the framework of the MSSM by using the Z-pole data, the m_W measurements, and low-energy neutral-current data. Our parameter sets are chosen to be in accordance with the region inside the 99% CL contour on the S_Z-T_Z plane presented in [17].

In cases without sfermion mixing, it is expected that lighter sfermions give larger one-loop contributions while heavy sfermions tend to decouple from the observables. We examine the cross section under this situation by introducing three cases, specified as A, B, C in Table 1. Another interesting situation is the case with large $\tilde{t}_L$-$\tilde{t}_R$ mixing. The magnitude of the mixing is determined by the off-diagonal part of the $\tilde{t}$-mass matrix, especially X_t (see Appendix A). To study the cross section in this situation, we select three parameter sets (Case 1, 2, 3 in Table 2), in which the maximal $\tilde{t}_L$-$\tilde{t}_R$ mixing occurs with the mixing angle $\theta_{\tilde{t}} \sim 45^\circ$ and a light $\tilde{t}_1$ with $m_{\tilde{t}_1} \sim 100$ GeV.

3.2 Partonic Cross Section

Before proceeding to the hadronic cross section, $pp \to W^- H^+$, we want to illustrate the partonic cross section of the subprocess $gg \to W^- H^+$ numerically. Although the partonic process is not accessible experimentally, it is useful for understanding the features of the hadronic cross section, in particular its dependence on the MSSM parameters. For gluon-fusion processes, the threshold region ($\sqrt{\hat{s}} \sim m_W + m_{H^\pm}$), where gluon pairs are most numerous in proton collisions, gives the dominant contribution to the hadronic cross section. Not intending completeness, we display here only one parameter set (Case 1 of Table 2) for the squark sector as an example.

In Figure 1 the integrated partonic cross section is shown as a function of $\sqrt{\hat{s}}$ for a sequence of $m_{H^\pm}$ values. Each plot displays three curves: the cross section evaluated from all (solid lines), only squark- (dotted lines) and only quark-loop diagrams (dashed lines).

	Case A			**Case B**			**Case C**		
$M_{\tilde{Q}}$ [GeV]	250			300			350		
$M_{\tilde{U}}$ [GeV]	250			300			350		
$M_{\tilde{D}}$ [GeV]	250			300			350		
X_t [GeV]	0			0			0		
X_b [GeV]	0			0			0		
$\tan\beta$	1.5	6	30	1.5	6	30	1.5	6	30
$m_{\tilde{t}_1}$ [GeV]	303	300	300	345	343	343	390	387	387
$m_{\tilde{t}_2}$ [GeV]	304	303	303	346	345	345	390	390	389
$m_{\tilde{b}_1}$ [GeV]	250	251	251	300	301	301	350	351	351
$m_{\tilde{b}_2}$ [GeV]	253	257	257	302	306	306	352	355	355

Table 1: Choices for the the soft supersymmetry breaking parameters $M_{\tilde{Q}}, M_{\tilde{U}}, M_{\tilde{D}}, X_t$ and X_b without squark mixing (i.e. $X_t = X_b = 0$). For all cases, μ is fixed to be zero. The resulting spectrum of the third generation squark masses is also displayed.

The last case corresponds to the scenario where the squarks decouple.

For $m_{H^\pm} = 100\,\text{GeV}$ [Figure 1(a)] the cross section is mainly dominated by the quark-loop diagrams. The $\tilde{b}\tilde{b}$ thresholds at $\sqrt{\hat{s}} \sim 2m_{\tilde{b}_1} \sim 2m_{\tilde{b}_2}$ from the squark-box diagrams are visible. Nevertheless, the $\tilde{b}\tilde{b}$ thresholds turn out to be of less importance for the hadronic cross section, because they are too far off the threshold of the associated H^+W^- production. Another effect of the squark-loop diagrams is present near the production threshold, where the tail of the $\tilde{t}_1\tilde{t}_1$-threshold still has influence and gives rise to a slightly enhanced hadronic cross section with respect to the squark decoupling case (see Figure 4).

At a charged-Higgs-boson mass of 210 GeV [Figure 1(b)] the cross section is largely dominated by the quark-loop diagrams. The peak corresponds to the $t\bar{t}$-threshold effect in the quark-box diagrams. A constructive squark-loop effect appears above the sbottom pair threshold, but this is negligible in the hadronic cross section.

For $m_{H^\pm} = 360\,\text{GeV}$ [Figure 1(c)] a novel enhancement of the partonic cross section occurs around the thresholds of sbottom pair production $\sqrt{\hat{s}} \sim 2m_{\tilde{b}_1} \sim 2m_{\tilde{b}_2}$, where the squark-loop contributions are dominant. Since the peak in the partonic cross section is near the W^-H^+ threshold where a lot of gluons are supplied, a large squark contribution appears also in the hadronic cross section, which corresponds to the local maximum of the hadronic cross section at around $m_{H^\pm} = 360$ GeV in Figure 4.

For $m_{H^\pm} = 450\,\text{GeV}$ [Figure 1(d)] there is neither a quark-pair nor a squark-pair threshold slightly above the W^-H^+ threshold, but the enhancement due to virtual squarks is still quite relevant.

	Case 1			**Case 2**			**Case 3**		
$M_{\tilde{Q}}$ [GeV]	250			300			350		
$M_{\tilde{U}}$ [GeV]	250			300			350		
$M_{\tilde{D}}$ [GeV]	250			300			350		
X_b [GeV]	0			0			0		
$\tan\beta$	1.5	6	30	1.5	6	30	1.5	6	30
X_t [GeV]	-470	-464	-463	-628	-621	-620	-813	-806	-806
$m_{\tilde{t}_1}$ [GeV]	101	100	101	101	101	101	102	102	102
$m_{\tilde{t}_2}$ [GeV]	417	414	414	479	476	476	542	540	540
$m_{\tilde{b}_1}$ [GeV]	251	251	251	300	301	301	350	351	351
$m_{\tilde{b}_2}$ [GeV]	253	257	257	302	306	306	352	355	355
$\theta_{\tilde{t}}$ [°]	44.9	44.7	44.7	44.9	44.8	44.8	44.9	44.8	44.8

Table 2: Choices for the the soft supersymmetry breaking parameters $M_{\tilde{Q}}, M_{\tilde{U}}, M_{\tilde{D}}, X_t$ and X_b for three values of $\tan\beta$ and the resulting spectrum of the third-generation squark masses and the mixing angle in the $\tilde{t}$-sector. For all cases, μ is fixed to be zero.

3.3 Hadronic Cross Section

The hadronic inclusive cross section for W^-H^+ production in proton-proton collisions at a total hadronic CM energy $\sqrt{S}$ can be written as a convolution [18]

$$\sigma(pp \to W^-H^+ + X) = \sum_{\{n,m\}} \int_{\tau_0}^1 d\tau \frac{d\mathcal{L}^{pp}_{nm}}{d\tau}\, \sigma_{nm\to W^-H^+}(\tau S, \alpha_S(\mu_R)) \tag{12}$$

with the parton luminosity

$$\frac{d\mathcal{L}^{pp}_{nm}}{d\tau} = \int_\tau^1 \frac{dx}{x} \frac{1}{1+\delta_{nm}} \Big[f_{n/p}(x,\mu_F) f_{m/p}(\frac{\tau}{x},\mu_F) + f_{m/p}(x,\mu_F) f_{n/p}(\frac{\tau}{x},\mu_F) \Big], \tag{13}$$

where $f_{n/p}(x,\mu_F)$ denotes the density of partons of type n in the proton carrying a fraction x of the proton momentum at the scale μ_F. In our case the sum over unordered pairs of partons $\{n,m\}$ reduces to two terms, i.e. there are two parton subprocesses contributing to inclusive W^-H^+ hadroproduction; gluon fusion and $b\bar{b}$-annihilation. Our main concern is the gluon-fusion process and the possible enhancement of the cross section through virtual squark effects with respect to the approximation of decoupling squarks. We will also compare the cross section for gluon fusion with the one for $b\bar{b}$-annihilation. The numerical evaluation has been carried out with the MRS(G) gluon distribution functions [19] and with the renormalization and factorization scale μ_R, μ_F chosen as equal.

The input parameters in the MSSM Higgs sector can be chosen to be $m_{H^\pm}$ and $\tan\beta$. Thus we study here the dependence of the hadronic cross section for W^-H^+ production

via gluon fusion on these two parameters for the different squark scenarios mentioned in chapter 3.1.

3.3.1 Unmixed sfermions

Figure 2 shows the variation of the hadronic cross section[6] with $m_{H^\pm}$ for the squark scenarios without mixing (cases A, B, C, see Table 1) and for two values of $\tan\beta$ (1.5 and 6). The cross section is decreasing rapidly with increasing charged-Higgs mass, except for the region around $m_{H^\pm} = 210$ GeV where a peak appears. The decrease of the cross section comes from the gluon luminosity, while the rise of the cross section in the peak area is due to the top-pair threshold in the quark-box diagrams, which gives rise to a sharp peak in the partonic cross section (see [Figure 1(b)]) at $\sqrt{\hat{s}} = 2m_t$ when the production threshold for the W^-H^+ is near $2m_t$. The squark scenarios without mixing (cases A, B, C, see Table 1) show generally an enhancement of the cross section with respect to the decoupling case of about 25% to 35% over the depicted $m_{H^\pm}$-range, except for the peak region between about 180 GeV and 250 GeV. Clearly, in this range the quark loop graphs dominate and the squark contribution corrects the quark-loop result only by a few percent.

The $\tan\beta$-dependence of the hadronic cross section is shown in Figure 3 for the non-mixing cases (case A, B, C, Table 1). The case in which all squarks decouple is also shown for comparison. One can see that the squark-loop contributions enhance the hadronic cross section for $\tan\beta$ values mainly below the point where the cross section takes its minimum, The enhancement is bigger for smaller $m_{H^\pm}$, e.g. 40% for squark-case A at $m_{H^\pm} = 100\,\text{GeV}$ and $\tan\beta = 5$. For $m_{H^\pm} = 100\,\text{GeV}$ and 300 GeV the enhancement is highest for the squark-case A with the lowest squark mass scale, and lowest for the squark-case C with the highest squark mass scale, while the situation is just the opposite at $m_{H^\pm} = 1000\,\text{GeV}$.

3.3.2 Maximal $\tilde{t}_L$-$\tilde{t}_R$ mixing

In Figure 4 the hadronic cross section for the squark scenarios with maximal $\tilde{t}_L$-$\tilde{t}_R$ mixing (cases 1, 2, 3, see Table 2) is shown as a function of $m_{H^\pm}$ for $\tan\beta = 1.5$ and 6, comparing the three squark scenarios with the squark decoupling case. The general feature of all three scenarios is that there is a second peak besides the one due to quark-box diagrams. This second peak originates from the squark-pair threshold effects in the squark-loop diagrams. If the W^-H^+ production threshold is somewhat below $2m_{\tilde{b}_{1(2)}}$, then the bottom-squark threshold of the box diagrams results in a pronounced peak in the parton cross section at

[6]With the 'hadronic cross section' we denote henceforth the cross section for W^-H^+ production via gluon fusion and take care that no confusion arises when the hadronic cross section for production of W^-H^+ via $b\bar{b}$-annihilation is addressed.

$\sqrt{\hat{s}} = 2m_{\tilde{b}_{1(2)}}$, which is even slightly higher than the peak due to quark loops (see Figure 1 (b) and (c)). The magnitude of the peak can be traced back to strongly enhanced couplings of the charged Higgs to $\tilde{t}_1\tilde{b}_1$ and $\tilde{t}_2\tilde{b}_1$ involving the non-diagonal entries of the $\tilde{t}$-mass matrix (see appendix C). It turns out that in the region of low $\tan\beta$ the contribution to the hadronic cross section from gluon fusion can be comparable and even slightly larger than the contribution from $b\bar{b}$ annihilation in the MSSM. This important feature is also shown in Figure 4, where the hadronic cross section for W^-H^+ production via $b\bar{b}$ annihilation for $\tan\beta = 1.5$ is also depicted for comparison.

The $\tan\beta$ dependence of the cross section in the large-mixing cases is shown in Figures 5 to 7. The squark cases with mixing are all rather similar in their behavior. Therefore we concentrate on Case 3 in Figure 7, as the most interesting example, for a more explicit discussion. In Figure 7, the hadronic cross section is displayed for three values of $m_{H^\pm}$ (100,470, 1000 GeV) in Case 3 (thick lines) and it is compared to the case of decoupling squarks (thin lines). From the logarithmic plot one can read off the fact that the enhancement due to squark effects in Case 3 with respect to the squark decoupling case keeps almost the same relative size for $\tan\beta$ values below the position of the minimum of the hadronic cross section. With further increasing $\tan\beta$ the enhancement diminishes slowly. Taking the case of $m_{H^\pm} = 470\,\mathrm{GeV}$ as an example, the magnitude of enhancement ranges from a factor of about 3 in the range $1 \leq \tan\beta \leq 10$ to 1.1 at $\tan\beta = 50$. In addition, there is a thin dot-dashed line in Figure 7 showing the hadronic cross section which originates only from the $b\bar{b}$-annihilation subprocess for the most interesting $m_{H^\pm}$-value of 470 GeV, where the contribution by gluon fusion to the inclusive hadron process gets as important as the one by $b\bar{b}$-annihilation for $\tan\beta = 1.5$ (see Figure 4). It turns out that this special feature in the large mixing cases is valid for small values of $\tan\beta$. The range of validity is limited from above roughly by the position of the minimum of the hadronic cross section originating only from $b\bar{b}$-annihilation, which is at $\tan\beta \approx 5$ in the case considered here. This is because for $\tan\beta$ greater than 5, the $b\bar{b}$-annihilation cross section is again rising, while the gluon fusion cross section has not approached its minimum yet.

The figures discussed in this paper are based on calculations assuming stable virtual particles, i.e. the finite widths of quarks and squarks have been neglected. This treatment is a resonable approximation since the widths of the heavy quarks and squarks are small compared to their masses. The widths of the squarks depend on the mass spectrum of the gauginos, which determine the kinematically allowed squark-decay channels but otherwise do not enter our calculation. For example, the light sbottom, which plays the crucial role in the threshold effects in the squark-box amplitudes, has a width of the order of 1 GeV, or much less if the decay channel $\tilde{b}_1 \to t\chi^-$ is kinematically closed (see e.g. [22]).

For a quantitative statement, we have estimated the finite-width effects for the squarks

and the top quark in our calculation. Taking into account a finite squark width yields a slight reduction of the threshold peak in the hadronic cross section (Figure 4) and no change off the peak. Specifically, we get a reduction of the peak value displayed in Figure 4 of 1 to 3 % in the various scanarios for squark widths of 0.1 GeV and of about 10 % for 1 GeV, almost independent of $\tan\beta$. The inclusion of the top quark width results in a reduction of 9 % for $\tan\beta = 1.5$ and 18 % for $\tan\beta = 6$ of the threshold peak located at $m_{H^\pm} = 210$ GeV in Figure 4.

4 Conclusions

We have discussed the charged-Higgs-boson production process associated with a W boson at hadron colliders. The hadronic cross section from the subprocess $gg \to W^- H^+$ has been calculated in the MSSM and the squark-loop contributions examined in comparison with the quark-loop effects for various MSSM parameters, which are chosen respecting bounds from the electroweak precision measurement and the squark direct search. We find that the squark (stop and sbottom) loop effects can be of about the same order as the t-b loop effects. In addition, for the maximum mixing between $\tilde{t}_L$ and $\tilde{t}_R$ with the mixing angle $\theta_t \sim \pi/4$, the hadronic cross section from $gg \to W^\pm H^\mp$ is extensively enhanced by the threshold effects of $\tilde{t}_1$ and $\tilde{b}_{1,2}$, where $\tilde{t}_1$ is the lighter stop. Therefore, the hadronic cross section via gluon fusion can reach the size of the cross section via the tree $b\overline{b}$ annihilation subprocess for smaller $\tan\beta$.

Acknowledgement.

This work was supported in part by the Alexander von Humboldt Foundation and by the Deutsche Forschungsgemeinschaft. Parts of the calculations have been performed on the QCM cluster at the University of Karlsruhe, supported by the DFG-Forschergruppe "Quantenfeldtheorie, Computeralgebra und Monte-Carlo-Simulation".

Appendix

A Squark masses and mixing

Squarks are introduced as the super-partners of quarks, so that there are three generations of isospin-doublets and -singlets corresponding to the quarks. The scalar partners of the L- and R-chiral quarks, in general, mix to form the mass eigenstates.

For the third generation of squarks, the mass-squared matrices in the L-R basis have the form

$$M_{\tilde{t}}^2 = \begin{pmatrix} M_{\tilde{Q}}^2 + m_t^2 + m_Z^2(\frac{1}{2} - e_t s_w^2)\cos 2\beta & m_t X_t \\ m_t X_t & M_{\tilde{U}}^2 + m_t^2 + m_Z^2 e_t s_w^2 \cos 2\beta \end{pmatrix} , \tag{14}$$

and

$$M_{\tilde{b}}^2 = \begin{pmatrix} M_{\tilde{Q}}^2 + m_b^2 + m_Z^2(-\frac{1}{2} - e_b s_w^2)\cos 2\beta & m_b X_b \\ m_b X_b & M_{\tilde{D}}^2 + m_b^2 + m_Z^2 e_b s_w^2 \cos 2\beta \end{pmatrix} , \tag{15}$$

where

$$X_t = A_t - \mu \cot\beta, \tag{16}$$

$$X_b = A_b - \mu \tan\beta. \tag{17}$$

For squarks of the first two generation, the mass matrices are obtained analogously. In Eqs. (14) and (15), the symbols e_t and e_b denote the electric charge of top- and bottom-quarks; μ is the supersymmetric Higgs mass parameter, $M_{\tilde{Q}}$ the soft-breaking mass parameter for the squark iso-doublet $(\tilde{t}_L, \tilde{b}_L)$, and $M_{\tilde{U}}$ and $M_{\tilde{D}}$ are the soft-breaking mass parameters for the iso-singlets $\tilde{t}_R$ and $\tilde{b}_R$. They can be different for each generation, but for simplicity we will assume equal values for all generations in our numerical analysis. A_t and A_b are the parameters of the soft-breaking scalar three-point interactions of top- and bottom-squarks with the Higgs fields.

We restrict our analysis to real parameters, so that the mass matrices for sfermions ($\tilde{f}_L$ and $\tilde{f}_R$) are real and can be diagonalized by introducing the mixing angles $\theta_{\tilde{f}}$. The mass eigenstates $\tilde{f}_1$ and $\tilde{f}_2$ are obtained as

$$\begin{pmatrix} \tilde{f}_1 \\ \tilde{f}_2 \end{pmatrix} = \begin{pmatrix} \cos\theta_{\tilde{f}} & -\sin\theta_{\tilde{f}} \\ \sin\theta_{\tilde{f}} & \cos\theta_{\tilde{f}} \end{pmatrix} \begin{pmatrix} \tilde{f}_L \\ \tilde{f}_R \end{pmatrix} .$$

The off-diagonal parts in the mass-squared matrices (14),(15) are proportional to the fermion masses. Therefore, the mixing effects are important mainly for third generation squarks.

B Helicity amplitudes

In the analytic expressions for the helicity amplitudes scalar 3- and 4-point functions appear for which the following conventions and shorthand notations are introduced:

$$C_0^{lm,ABC} = \frac{1}{i\pi^2}\int d^4k \frac{1}{[k^2-m_A^2][(k+p_l)^2-m_B^2][(k+p_l+p_m)^2-m_C^2]} ,$$
$$D_0^{klm,ABCD} = \frac{1}{i\pi^2}\int d^4k \frac{1}{[k^2-m_A^2][(k+p_k)^2-m_B^2][(k+p_k+p_l)^2-m_C^2][(k+p_k+p_l+p_m)^2-m_D^2]} .$$

Furthermore, in the box amplitudes tensor coefficients appear, where the upper indices denote momenta and masses in the same way as above. The lower index of the tensor coefficients gives the number in the tensor decomposition and corresponds precisely to the naming in [20] except for the fact that the Minkowski metric is used as implemented in the Fortran package AAFF [21], which has been used in the numerical evaluation. To match the definition of the loop integrals the external momenta are all chosen as incoming. Thus we have the following translation to the definition of section 2.1:

$$p_1 = k \qquad p_2 = \bar{k} \qquad p_3 = -p \qquad p_4 = -\bar{p} .$$

In some C-functions a sum of two momenta $p_l + p_k$ appears as one of the momentum arguments, which is then denoted by (lk). The amplitude for $gg \to W^-H^+$ is divided into contributions from quark and squark loops and further into triangle-type and box-type diagrams:

$$\mathcal{M}_{\sigma\bar{\sigma}\lambda} = \mathcal{M}^{q,\triangle}_{\sigma\bar{\sigma}\lambda} + \mathcal{M}^{q,\square}_{\sigma\bar{\sigma}\lambda} + \mathcal{M}^{\tilde{q},\triangle}_{\sigma\bar{\sigma}\lambda} + \mathcal{M}^{\tilde{q},\square}_{\sigma\bar{\sigma}\lambda} \tag{18}$$

Regarding the squark loops, we include the 2-point loops in the triangle contribution and the triangles without Higgs exchange in the box contribution.

B.1 Quark contributions

Triangle contributions

$$\mathcal{M}^{q,\triangle}_{\sigma\bar{\sigma}\lambda} = (K_{1\,\sigma\bar{\sigma}\lambda} + K_{2\,\sigma\bar{\sigma}\lambda})T_1^{q,\triangle} + (K_{10\,\sigma\bar{\sigma}\lambda} + K_{11\,\sigma\bar{\sigma}\lambda})T_2^{q,\triangle} \tag{19}$$

$$T_1^{q,\triangle} = \frac{i\,g_S^2}{\pi^2}\Bigg[g[H^0H^\pm W^\mp] \times$$
$$\times \left(\frac{m_t\, g_s[H^0tt]}{\hat{s} - {m_H}^2}\left((\frac{\hat{s}}{2} - 2\,{m_t}^2)\, C_0^{12,ttt} - 1 \right) + \frac{m_b\, g_s[H^0bb]}{\hat{s} - {m_H}^2}\left((\frac{\hat{s}}{2} - 2\,{m_b}^2)\, C_0^{12,bbb} - 1 \right) \right)$$
$$+ g[h^0H^\pm W^\mp] \left(\frac{m_t\, g_s[h^0tt]}{\hat{s} - {m_h}^2}\left((\frac{\hat{s}}{2} - 2\,{m_t}^2)\, C_0^{12,ttt} - 1 \right) + \frac{m_b\, g_s[h^0bb]}{\hat{s} - {m_h}^2}\left((\frac{\hat{s}}{2} - 2\,{m_b}^2)\, C_0^{12,bbb} - 1 \right) \right) \Bigg]$$

$$T_2^{q,\triangle} = \frac{g_S^2\, g[A^0 H^\pm W^\mp]}{\pi^2\,(\hat{s} - {m_A}^2)} \Big(m_t\, g_p[A^0\, tt]\; C_0^{12,ttt} + m_b\, g_p[A^0\, bb]\; C_0^{12,bbb} \Big)$$

The universal helicity factors $K_{i\,\sigma\bar{\sigma}\lambda}$ are listed below in appendix B.3.

Box contributions

$$\mathcal{M}^{q,\Box}_{\sigma\bar{\sigma}\lambda} = \sum_{i=1}^{24} K_{i\,\sigma\bar{\sigma}\lambda} T_i^{q,\Box} \tag{20}$$

$$\begin{aligned}
T_1^{q,\Box} &= \frac{i\, g_S^2\, g_2}{4\sqrt{2}\pi^2} \Big[m_t\, g_+ \Big(R_1 + D_{12}^{132,bbtt} + D_{22}^{132,bbtt} - D_{22}^{231,bbtt} - D_{13}^{124,tttb} - D_{13}^{214,tttb} + D_{23}^{123,bbbt} \\
&\quad - D_{23}^{124,tttb} + D_{23}^{213,bbbt} - D_{23}^{214,tttb} \Big) + m_b\, g_- \Big(R_1 + D_0^{132,bbtt} + 4\, D_{12}^{132,bbtt} + D_{12}^{231,bbtt} \\
&\quad + D_{22}^{231,bbtt} + 3\, D_{22}^{132,bbtt} + D_{13}^{123,bbbt} + D_{13}^{213,bbbt} + 3\, D_{23}^{123,bbbt} + D_{23}^{124,tttb} + 3\, D_{23}^{213,bbbt} + D_{23}^{214,tttb} \Big) \Big] \\
T_2^{q,\Box} &= T_1^{q,\Box}(p_1 \leftrightarrow p_2) \\
R_1 &= 2\,(D_{24}^{132,bbtt} + D_{26}^{231,bbtt} - D_{33}^{124,tttb} - D_{33}^{214,tttb} + D_{36}^{132,bbtt} + D_{37}^{123,bbbt} + D_{37}^{124,tttb} + D_{38}^{231,bbtt} \\
&\quad + D_{39}^{213,bbbt} + D_{39}^{214,tttb}) \\
T_3^{q,\Box} &= \frac{i\, g_S^2\, g_2}{2\sqrt{2}\pi^2} \frac{1}{8} \Big[m_t\, g_+ \Big((-\hat{u} + m_W^2) D_0^{214,tttb} - D_0^{123,bbbt}\, \hat{s} + (\,\hat{t} - m_{H^\pm}^2\,)\,(D_0^{132,bbtt} - D_0^{124,tttb}) \\
&\quad + 4(D_{27}^{132,bbtt} + D_{27}^{213,bbbt} - D_{27}^{214,tttb} - D_{27}^{231,bbtt} + D_{27}^{123,bbbt} - D_{27}^{124,tttb}) \\
&\quad + 2\,(C_0^{34,tbt} - C_0^{34,btb}) + R_2 \Big) + m_b\, g_- \Big((m_{H^\pm}^2 - 2\,\hat{s} - \hat{t}\,)\, D_0^{123,bbbt} - D_0^{132,bbtt}\, \hat{s} \\
&\quad - (\,-\hat{t} + \hat{s} + m_{H^\pm}^2\,)\, D_0^{213,bbbt} - D_0^{124,tttb}\, \hat{s} - (\,-\hat{u} + m_W^2\,)\, D_0^{231,bbtt} \\
&\quad + 4(3D_{27}^{132,bbtt} + 3D_{27}^{213,bbbt} + D_{27}^{214,tttb} + D_{27}^{231,bbtt} + 3D_{27}^{123,bbbt} + D_{27}^{124,tttb}) \\
&\quad - 2\,(C_0^{34,tbt} + 3\, C_0^{34,btb}) + R_2 \Big) \Big] \\
T_4^{q,\Box} &= T_3^{q,\Box}(p_1 \leftrightarrow p_2) \\
R_2 &= \hat{s}(-D_{11}^{124,tttb} - D_{11}^{123,bbbt} - D_{11}^{132,bbtt} - D_{12}^{213,bbbt} - D_{12}^{214,tttb} + D_{13}^{214,tttb} + D_{13}^{124,tttb} - D_{13}^{231,bbtt}) \\
&\quad + 8(D_{311}^{123,bbbt} + D_{311}^{132,bbtt} + D_{311}^{124,tttb} + D_{312}^{214,tttb} + D_{312}^{213,bbbt} + D_{313}^{231,bbtt} - D_{313}^{214,tttb} - D_{313}^{124,tttb}) \\
&\quad - 4(\, C_{11}^{(12)3,bbt} + \, C_{11}^{(12)4,ttb} - \, C_{12}^{(12)4,ttb}) \\
T_5^{q,\Box} &= \frac{i\, g_S^2\, g_2}{2\sqrt{2}\pi^2} \frac{1}{8} \Big[m_t\, g_+ \Big(\hat{s}\,(-\, D_0^{214,tttb} + D_0^{124,tttb} + D_{12}^{132,bbtt} + D_{13}^{123,bbbt} + D_{13}^{213,bbbt}) \\
&\quad - (\,2\, m_W^2 - \hat{s} - 2\,\hat{t}\,)\,(D_{13}^{124,tttb} + D_{13}^{214,tttb} - D_{12}^{231,bbtt}) + R_3^+ \Big) \\
&\quad + m_b\, g_- \Big(\hat{s}\,(D_0^{123,bbbt} - D_0^{213,bbbt} + D_0^{231,bbtt} - D_{13}^{124,tttb} - D_{13}^{214,tttb} - D_{12}^{231,bbtt}) \\
&\quad + (\,2\, m_W^2 - \hat{s} - 2\,\hat{t}\,)\,(D_0^{132,bbtt} + D_{12}^{132,bbtt} + D_{13}^{123,bbbt} + D_{13}^{213,bbbt}) + R_3^-) \Big) \Big] \\
T_6^{q,\Box} &= T_5^{q,\Box}(p_1 \leftrightarrow p_2)
\end{aligned}$$

$$
\begin{aligned}
R_3^{\pm} &= 8\,(D_{312}^{132,bbtt} + D_{312}^{231,bbtt} + D_{313}^{123,bbbt} + D_{313}^{213,bbbt} - D_{313}^{214,tttb} - D_{313}^{124,tttb} + D_{27}^{132,bbtt}) \\
&\quad - 2\,(2\,C_{12}^{2(13),bbt} - C_{12}^{24,ttb} + C_0^{24,ttb} + C_{11}^{(13)2,btt}) \mp 2\,(C_0^{23,ttb} + C_{12}^{2(14),ttb} + C_{11}^{32,btt}) \\
T_7^{q,\Box} &= \frac{g_S^2\,g_2}{2\sqrt{2}\pi^2}\frac{1}{4}\Big[m_t\,g_+\Big(R_4 + D_{13}^{132,bbtt}\Big) \\
&\quad + m_b\,g_-\Big(R_5 - D_0^{123,bbbt} + D_0^{213,bbbt} - D_{11}^{123,bbbt} + D_{11}^{132,bbtt} + D_{11}^{213,bbbt}\Big)\Big] \\
T_8^{q,\Box} &= \frac{g_S^2\,g_2}{2\sqrt{2}\pi^2}\frac{1}{4}\Big[m_t\,g_+\Big(-R_4(p_1\leftrightarrow p_2) - D_{13}^{132,bbtt}\Big) + m_b\,g_-\Big(-R_5(p_1\leftrightarrow p_2) - D_{11}^{231,bbtt}\Big)\Big] \\
R_4 &= -D_0^{214,tttb} - D_{11}^{214,tttb} - D_{12}^{124,tttb} - D_{12}^{231,bbtt} - D_{13}^{123,bbbt} + D_{13}^{124,tttb} \\
R_5 &= D_0^{132,bbtt} + D_{11}^{231,bbtt} - D_{12}^{231,bbtt} + D_{13}^{124,tttb} \\
T_9^{q,\Box} &= \frac{g_S^2\,g_2}{2\sqrt{2}\pi^2}\frac{1}{4}\Big[m_t\,g_+\Big(-\,D_{11}^{124,tttb} + D_{11}^{214,tttb} + D_{12}^{124,tttb} - D_{12}^{214,tttb}\Big) \\
&\quad + m_b\,g_-\Big(D_{11}^{123,bbbt} - D_{11}^{213,bbbt} - D_{13}^{123,bbbt} + D_{13}^{213,bbbt}\Big)\Big] \\
T_{10}^{q,\Box} &= \frac{g_S^2\,g_2}{2\sqrt{2}\pi^2}\frac{1}{4}\Big[m_t\,g_+\Big(R_6 + D_{12}^{124,tttb} - D_{12}^{214,tttb} + D_{13}^{214,tttb} + D_{23}^{124,tttb} + D_{24}^{124,tttb} - D_{25}^{124,tttb} \\
&\quad - D_{26}^{124,tttb}\Big) + m_b\,g_-\Big(R_7 + R_8\Big)\Big] \\
T_{11}^{q,\Box} &= \frac{g_S^2\,g_2}{2\sqrt{2}\pi^2}\frac{1}{4}\Big[m_t\,g_+\Big(R_6(p_1\leftrightarrow p_2) + D_{13}^{214,tttb} + D_{22}^{124,tttb} + D_{23}^{124,tttb} - 2\,D_{26}^{124,tttb}\Big) \\
&\quad + m_b\,g_-\Big(R_7(p_1\leftrightarrow p_2) + R_8\Big)\Big] \\
R_6 &= -D_{11}^{124,tttb} + D_{11}^{132,bbtt} + D_{12}^{123,bbbt} + D_{12}^{213,bbbt} + D_{21}^{132,bbtt} + D_{22}^{213,bbbt} + D_{24}^{123,bbbt} + D_{25}^{231,bbtt} \\
R_7 &= D_0^{123,bbbt} + D_0^{132,bbtt} + D_0^{213,bbbt} + 2\,D_{11}^{123,bbbt} + D_{11}^{132,bbtt} + D_{12}^{124,tttb} + 2\,D_{12}^{213,bbbt} + D_{12}^{214,tttb} \\
&\quad + D_{21}^{123,bbbt} + D_{22}^{214,tttb} + D_{23}^{124,tttb} + D_{23}^{214,tttb} + D_{23}^{231,bbtt} + D_{24}^{124,tttb} + D_{24}^{213,bbbt} - D_{25}^{124,tttb} \\
&\quad + D_{25}^{132,bbtt} - D_{26}^{124,tttb} - 2\,D_{26}^{214,tttb} \\
R_8 &= -D_{13}^{124,tttb} + D_{13}^{132,bbtt} - D_{13}^{214,tttb} + D_{13}^{231,bbtt} \\
T_{12}^{q,\Box} &= \frac{g_S^2\,g_2}{2\sqrt{2}\pi^2}\frac{1}{4}\Big[m_t\,g_+\Big(R_9 + R_{10} + D_0^{124,tttb} - D_0^{214,tttb} + D_{11}^{124,tttb} - D_{11}^{214,tttb}\Big) \\
&\quad + m_b\,g_-\Big(R_{11}\Big)\Big] \\
T_{13}^{q,\Box} &= \frac{g_S^2\,g_2}{2\sqrt{2}\pi^2}\frac{1}{4}\Big[m_t\,g_+\Big(-R_9(p_1\leftrightarrow p_2) + R_{10} - D_{23}^{124,tttb} - 2\,D_{23}^{214,tttb} + 2\,D_{26}^{214,tttb}\Big) \\
&\quad + m_b\,g_-\Big(-R_{11}(p_1\leftrightarrow p_2)\Big)\Big] \\
R_9 &= -D_{12}^{124,tttb} - D_{12}^{132,bbtt} + D_{13}^{124,tttb} + 2D_{13}^{132,bbtt} + D_{13}^{213,bbbt} + 2D_{25}^{213,bbbt} - 2D_{25}^{214,tttb} + 2D_{26}^{132,bbtt} \\
R_{10} &= D_{23}^{124,tttb} + 2D_{23}^{214,tttb} - D_{24}^{132,bbtt} + D_{24}^{231,bbtt} + D_{26}^{123,bbbt} - D_{26}^{124,tttb} - D_{26}^{213,bbbt} \\
R_{11} &= D_0^{132,bbtt} + D_0^{213,bbbt} + D_{11}^{132,bbtt} + D_{11}^{213,bbbt} + D_{11}^{231,bbtt} + D_{12}^{231,bbtt} + D_{13}^{123,bbbt} \\
&\quad + D_{13}^{132,bbtt} + D_{13}^{213,bbbt} - D_{13}^{214,tttb} - D_{13}^{231,bbtt} + D_{23}^{124,tttb} + D_{23}^{214,tttb} + 2D_{24}^{231,bbtt} - D_{25}^{123,bbbt} \\
&\quad + D_{25}^{213,bbbt} - 2D_{25}^{214,tttb} + 2D_{26}^{123,bbbt} - D_{26}^{124,tttb} + D_{26}^{132,bbtt} + D_{26}^{214,tttb} - D_{26}^{231,bbtt}
\end{aligned}
$$

$$
\begin{aligned}
T_{14}^{q,\Box} &= \frac{g_S^2\, g_2}{2\sqrt{2}\pi^2}\frac{1}{4}\Big[m_t\, g_+\Big(- D_0^{124,tttb} - D_{11}^{124,tttb} + D_{11}^{132,bbtt} - D_{12}^{214,tttb} + D_{13}^{123,bbbt} + D_{13}^{214,tttb} \\
&+ D_{21}^{132,bbtt} - D_{22}^{214,tttb} + D_{23}^{124,tttb} - D_{23}^{214,tttb} + D_{25}^{123,bbbt} - D_{25}^{124,tttb} + 2\, D_{26}^{214,tttb} + D_{26}^{231,bbtt}\Big) \\
&+ m_b\, g_-\Big(D_0^{123,bbbt} + D_0^{132,bbtt} + 2\, D_{11}^{123,bbbt} + D_{11}^{132,bbtt} + D_{12}^{132,bbtt} + D_{12}^{213,bbbt} - D_{13}^{124,tttb} \\
&+ D_{21}^{123,bbbt} + D_{23}^{124,tttb} + D_{24}^{132,bbtt} - D_{25}^{124,tttb} + D_{26}^{213,bbbt}\Big)\Big] \\
T_{15}^{q,\Box} &= \frac{g_S^2\, g_2}{2\sqrt{2}\pi^2}\frac{1}{4}\Big[m_t\, g_+\Big(D_{11}^{124,tttb} - D_{12}^{124,tttb} - D_{12}^{214,tttb} + D_{12}^{231,bbtt} + D_{13}^{123,bbbt} + D_{13}^{214,tttb} + D_{23}^{124,tttb} \\
&- D_{23}^{214,tttb} - D_{24}^{214,tttb} + D_{24}^{231,bbtt} + D_{25}^{132,bbtt} + D_{25}^{214,tttb} + D_{26}^{123,bbbt} - D_{26}^{124,tttb} + D_{26}^{214,tttb}\Big) \\
&+ m_b\, g_-\Big(D_0^{123,bbbt} + D_{11}^{123,bbbt} + D_{11}^{213,bbbt} + D_{12}^{123,bbbt} - D_{13}^{124,tttb} + D_{13}^{132,bbtt} \\
&+ D_{23}^{124,tttb} + D_{24}^{123,bbbt} + D_{25}^{213,bbbt} - D_{26}^{124,tttb} + D_{26}^{132,bbtt}\Big)\Big] \\
T_{16}^{q,\Box} &= \frac{g_S^2\, g_2}{2\sqrt{2}\pi^2}\frac{1}{4}\Big[m_t\, g_+\Big(D_{12}^{132,bbtt} + D_{13}^{124,tttb} + 2\, D_{13}^{214,tttb} + 2\, D_{22}^{132,bbtt} + D_{22}^{231,bbtt} + D_{23}^{123,bbbt} \\
&+ D_{23}^{124,tttb} + 2\, D_{23}^{213,bbbt} + 3\, D_{23}^{214,tttb} - D_{24}^{132,bbtt} - D_{26}^{214,tttb}\Big) \\
&+ m_b\, g_-\Big(D_0^{132,bbtt} + 2\, D_{12}^{132,bbtt} + 2\, D_{12}^{231,bbtt} + D_{13}^{123,bbbt} + D_{13}^{213,bbbt} + D_{22}^{132,bbtt} + 2\, D_{22}^{231,bbtt} \\
&+ 2\, D_{23}^{123,bbbt} + D_{23}^{124,tttb} + D_{23}^{213,bbbt} + 2\, D_{23}^{214,tttb} - D_{25}^{123,bbbt}\Big)\Big] \\
T_{17}^{q,\Box} &= \frac{g_S^2\, g_2}{2\sqrt{2}\pi^2}\frac{1}{4}\Big[m_t\, g_+\Big(D_{12}^{132,bbtt} + D_{13}^{124,tttb} + D_{22}^{231,bbtt} + D_{23}^{123,bbbt} + D_{23}^{124,tttb} - D_{23}^{214,tttb} \\
&+ D_{24}^{132,bbtt} + D_{26}^{214,tttb}\Big) + m_b\, g_-\Big(D_0^{132,bbtt} + 2\, D_{12}^{132,bbtt} + D_{13}^{123,bbbt} + D_{13}^{213,bbbt} + D_{22}^{132,bbtt} \\
&+ D_{23}^{124,tttb} + D_{23}^{213,bbbt} + D_{25}^{123,bbbt}\Big)\Big] \\
T_{18}^{q,\Box} &= \frac{g_S^2\, g_2}{2\sqrt{2}\pi^2}\frac{1}{8}\Big[m_t\, g_+\Big(- \ m_b\, m_t\, (D_0^{123,bbbt} + D_0^{213,bbbt} + 2\, D_0^{132,bbtt} + 2\, D_0^{124,tttb} + D_{11}^{123,bbbt}) \\
&+ (\ {m_b}^2 - {m_t}^2 + m_{H\pm}^2\ )\, (D_0^{132,bbtt} + D_{11}^{132,bbtt} - D_{12}^{214,tttb} + D_{13}^{214,tttb}) + (\ \hat{u} - m_{H\pm}^2\ )\, D_{13}^{231,bbtt} \\
&+ {m_b}^2\, (2\, D_0^{123,bbbt} - 2\, D_0^{231,bbtt} + D_0^{124,tttb}) - ({m_t}^2 - m_{H\pm}^2) D_0^{124,tttb} \\
&+ (C_{11}^{(12)4,ttb} - C_{12}^{(12)4,ttb} - C_0^{13,ttb} + 2\, C_0^{24,ttb} - C_0^{12,ttt} - C_{12}^{21,ttt} \\
&- 4\, D_{27}^{132,bbtt} - 4\, D_{27}^{213,bbbt} + 2\, D_{27}^{123,bbbt} + 2\, D_{27}^{231,bbtt} + R_9)\Big) \\
&+ m_b\, g_-\Big((\ \hat{u} + {m_b}^2\ )\, (D_0^{123,bbbt} + D_{11}^{123,bbbt}) - (\ \hat{u} - m_{H\pm}^2\ )\, (D_0^{132,bbtt} + D_{11}^{132,bbtt}) \\
&- (\ {m_b}^2 - m_{H\pm}^2\ )\, D_0^{213,bbbt} + (\ \hat{t} - m_{H\pm}^2\ )\, D_{13}^{231,bbtt} \\
&+ (C_0^{14,ttb} + C_0^{24,ttb} - C_{11}^{12,bbb} - C_{12}^{(23)1,btt} - 2\, C_0^{12,bbb} + C_{12}^{31,btt} \\
&+ C_0^{24,bbt} - C_0^{13,bbt} + 2\, D_{27}^{132,bbtt} + 2\, D_{27}^{213,bbbt} - 4\, D_{27}^{231,bbtt} - 4\, D_{27}^{123,bbbt} + R_9)\Big) \\
&+ 2\, {m_t}^2\, m_b\, g_s[H^+\,\mathrm{out}, t\,\mathrm{in}, b\,\mathrm{out}]\, \Big(D_0^{123,bbbt} + 2\, D_0^{124,tttb} + 2\, D_0^{132,bbtt} + D_0^{213,bbbt} + D_{11}^{123,bbbt}\Big)\Big] \\
R_9 &= -C_{12}^{14,ttb} + C_{12}^{24,ttb} + C_{11}^{(13)2,btt} - C_{12}^{2(13),bbt} + C_{11}^{14,ttb} - 4\, D_{27}^{214,tttb} + 2\, D_{27}^{124,tttb}
\end{aligned}
$$

$$
\begin{aligned}
T_{19}^{q,\Box} &= \frac{g_S^2\, g_2}{2\sqrt{2}\pi^2}\frac{1}{4}\Big[m_t\, g_+\Big(-\ D_0^{124,tttb} - D_{11}^{124,tttb} - D_{11}^{214,tttb} - D_{12}^{132,bbtt} + D_{13}^{132,bbtt} - D_{13}^{213,bbbt} \\
&\quad + D_{13}^{214,tttb} - D_{23}^{214,tttb} - D_{24}^{132,bbtt} - D_{24}^{214,tttb} + D_{25}^{132,bbtt} + D_{25}^{214,tttb} - D_{26}^{213,bbbt} + D_{26}^{214,tttb}\Big) \\
&\quad + m_b\, g_-\Big(-\ D_{11}^{123,bbbt} + D_{12}^{123,bbbt} + D_{13}^{214,tttb} - D_{13}^{231,bbtt} \\
&\quad - D_{23}^{214,tttb} + D_{24}^{123,bbbt} - D_{25}^{123,bbbt} + D_{26}^{214,tttb} - D_{26}^{231,bbtt}\Big)\Big] \\
T_{20}^{q,\Box} &= \frac{g_S^2\, g_2}{2\sqrt{2}\pi^2}\frac{1}{4}\Big[m_t\, g_+\Big(-\ D_{11}^{214,tttb} - D_{13}^{213,bbbt} + D_{13}^{214,tttb} - D_{21}^{214,tttb} + D_{23}^{132,bbtt} - D_{23}^{214,tttb} \\
&\quad - D_{25}^{213,bbbt} + 2\, D_{25}^{214,tttb} - D_{26}^{132,bbtt}\Big) + m_b\, g_-\Big(-\ D_0^{231,bbtt} - D_{11}^{231,bbtt} - D_{12}^{231,bbtt} \\
&\quad + D_{13}^{214,tttb} + D_{22}^{123,bbbt} - D_{23}^{214,tttb} - D_{24}^{231,bbtt} + D_{25}^{214,tttb} - D_{26}^{123,bbbt}\Big)\Big] \\
T_{21}^{q,\Box} &= \frac{g_S^2\, g_2}{2\sqrt{2}\pi^2}\frac{1}{4}\Big[m_t\, g_+\Big(D_{22}^{132,bbtt} + D_{23}^{213,bbbt} + D_{23}^{214,tttb} - D_{25}^{214,tttb} - D_{26}^{132,bbtt}\Big) \\
&\quad + m_b\, g_-\Big(D_0^{231,bbtt} + 2\, D_{12}^{231,bbtt} + D_{22}^{231,bbtt} + D_{23}^{123,bbbt} + D_{23}^{214,tttb} - D_{26}^{123,bbbt}\Big)\Big] \\
T_{22}^{q,\Box} &= \frac{g_S^2\, g_2}{2\sqrt{2}\pi^2}\frac{1}{4}\Big[m_t\, g_+\Big(2\, D_{12}^{231,bbtt} + 2\, D_{13}^{124,tttb} + 2\, D_{13}^{214,tttb} + D_{22}^{132,bbtt} + 2\, D_{22}^{231,bbtt} + 2\, D_{23}^{123,bbbt} \\
&\quad + 2\, D_{23}^{124,tttb} + D_{23}^{213,bbbt} + D_{23}^{214,tttb} + D_{25}^{214,tttb} + D_{26}^{132,bbtt}\Big) \\
&\quad + m_b\, g_-\Big(D_0^{231,bbtt} + 2\, D_{12}^{132,bbtt} + 2\, D_{12}^{231,bbtt} + 2\, D_{13}^{123,bbbt} + 2\, D_{13}^{213,bbbt} + 2\, D_{22}^{132,bbtt} \\
&\quad + D_{22}^{231,bbtt} + D_{23}^{123,bbbt} + 2\, D_{23}^{124,tttb} + 2\, D_{23}^{213,bbbt} + D_{23}^{214,tttb} + D_{26}^{123,bbbt}\Big)\Big] \\
T_{23}^{q,\Box} &= \frac{g_S^2\, g_2}{2\sqrt{2}\pi^2}\frac{1}{8}\Big[m_t\, g_+\Big(2\, {m_b}^2\, (D_0^{132,bbtt} + D_0^{213,bbbt}) + m_b\, m_t\, (2\, D_0^{231,bbtt} + 2\, D_0^{214,tttb} - D_{12}^{123,bbbt}) \\
&\quad + (\hat{u} - m_{H\pm}^2)\, (D_0^{231,bbtt} + D_{11}^{231,bbtt}) + (\, {m_b}^2 - {m_t}^2 + m_{H\pm}^2\,)\, (D_{13}^{132,bbtt} + D_{13}^{214,tttb} - D_{11}^{214,tttb}) \\
&\quad + (4\, D_{27}^{123,bbbt} - 2\, D_{27}^{213,bbbt} + 4\, D_{27}^{214,tttb} + 4\, D_{27}^{231,bbtt} - 2\, D_{27}^{132,bbtt} \\
&\quad + C_{11}^{(12)4,ttb} - C_{12}^{(12)4,ttb} - C_{11}^{21,ttt} - C_0^{24,bbt} - C_{11}^{2(13),bbt} + R_{10})\Big) \\
&\quad + m_b\, g_-\Big(2\, {m_b}^2\, D_0^{123,bbbt} + (\hat{u} - m_{H\pm}^2)\, (D_0^{123,bbbt} - D_{13}^{132,bbtt}) \\
&\quad + (\, \hat{t} - m_{H\pm}^2\,)\, (D_0^{231,bbtt} + D_{11}^{231,bbtt}) + (\, \hat{u} + {m_b}^2\,)\, D_{12}^{123,bbbt} \\
&\quad + (4\, D_{27}^{132,bbtt} - 2\, D_{27}^{214,tttb} - 2\, D_{27}^{231,bbtt} - 2\, D_{27}^{123,bbbt} + 4\, D_{27}^{213,bbbt} \\
&\quad - C_{11}^{(23)1,btt} - C_0^{24,ttb} + C_0^{24,bbt} - C_{12}^{32,btt} + C_0^{23,bbt} - C_{12}^{12,bbb} + C_{11}^{2(13),bbt} + R_{10})\Big) \\
&\quad + 2{m_t}^2\, m_b\, g_s[H^+\,\text{out}, t\,\text{in}, b\,\text{out}]\,\Big(D_{12}^{123,bbbt} - 2\, D_0^{231,bbtt} - 2\, D_0^{214,tttb}\Big)\Big] \\
R_{10} &= 4\, D_{27}^{124,tttb} - C_0^{14,ttb} - C_{12}^{14,ttb} + C_{12}^{24,ttb} - C_{11}^{24,ttb} + C_{12}^{(13)2,btt}
\end{aligned}
$$

$$
\begin{aligned}
T_{24}^{q,\Box} = \frac{g_S^2\, g_2}{2\sqrt{2}\pi^2}\frac{1}{8}\Big[& m_t\, g_+\Big(2\, {m_b}^2\, D_0^{132,bbtt} - 2\, {m_t}^2\, D_0^{214,tttb} + (\, {m_b}^2 - {m_t}^2 + m_{H\pm}^2\,)\, D_{12}^{132,bbtt} \\
& + (\, \hat{u} - m_{H\pm}^2\,)\, D_{12}^{231,bbtt} + (\, {m_b}^2 - {m_t}^2 - m_{H\pm}^2\,)\, D_{13}^{214,tttb} - \, m_t\, m_b\, D_{13}^{123,bbbt} \\
& - (C_0^{34,tbt} - 2\, C_0^{24,ttb} + C_{12}^{(12)4,ttb} + C_{12}^{2(13),bbt} - 6\, D_{27}^{214,tttb} + 6\, D_{27}^{132,bbtt} + R_{11})\Big) \\
& + m_b\, g_-\Big(2\, {m_b}^2\, D_0^{123,bbbt} - (\, \hat{u} - m_{H\pm}^2\,)\, (D_0^{132,bbtt} + D_{12}^{132,bbtt}) \\
& + (\, \hat{t} - m_{H\pm}^2\,)\, (D_0^{231,bbtt} + D_{12}^{231,bbtt}) + (\, \hat{u} + {m_b}^2\,)\, D_{13}^{123,bbbt} - (C_{11}^{(23)1,btt} - C_0^{34,btb} - C_0^{13,ttb} \\
& - C_{11}^{31,btt} + C_0^{23,ttb} - C_0^{24,ttb} + C_{11}^{32,btt} - C_{12}^{2(13),bbt} - C_0^{24,bbt} + 6\, D_{27}^{123,bbbt} + R_{11})\Big) \\
& + 2\, {m_t}^2\, m_b\, g_s[H^+\,\mathrm{out}, t\,\mathrm{in}, b\,\mathrm{out}]\, D_{13}^{123,bbbt}\Big] \\
R_{11} = {} & C_0^{14,ttb} - C_{11}^{(13)2,btt} + C_{12}^{14,ttb} - C_{12}^{24,ttb}
\end{aligned}
$$

Here the shorthand

$$
g_\pm = g_s[H^+\,\mathrm{out}, t\,\mathrm{in}, b\,\mathrm{out}] \pm g_p[H^+\,\mathrm{out}, t\,\mathrm{in}, b\,\mathrm{out}]
$$

has been used.

B.2 Squark contributions

Triangle contributions

$$
\mathcal{M}_{\sigma\bar{\sigma}\lambda}^{\tilde{q},\triangle} = (K_{1\,\sigma\bar{\sigma}\lambda} + K_{2\,\sigma\bar{\sigma}\lambda}) T_1^{\tilde{q},\triangle} \tag{21}
$$

$$
\begin{aligned}
T_1^{\tilde{q},\triangle} = \sum_{i=1}^{2} \frac{i\, g_S^2}{4\,\pi^2}\Big[& \frac{g[H^0 H^\pm W^\mp]}{\hat{s} - {m_H}^2} \times \\
& \times \Big(g[H^0 \tilde{t}_i \tilde{t}_i]\Big(1 + 2\, m_{\tilde{t}_i}^2\, C_0^{12,\tilde{t}_i\tilde{t}_i\tilde{t}_i}\Big) + g[H^0 \tilde{b}_i \tilde{b}_i]\Big(1 + 2\, m_{\tilde{b}_i}^2\, C_0^{12,\tilde{b}_i\tilde{b}_i\tilde{b}_i}\Big) \\
& + \frac{g[h^0 H^\pm W^\mp]}{\hat{s} - {m_h}^2}\Big(+ g[h^0 \tilde{t}_i \tilde{t}_i]\Big(1 + 2\, m_{\tilde{t}_i}^2\, C_0^{12,\tilde{t}_i\tilde{t}_i\tilde{t}_i}\Big) + g[h^0 \tilde{b}_i \tilde{b}_i]\Big(1 + 2\, m_{\tilde{b}_i}^2\, C_0^{12,\tilde{b}_i\tilde{b}_i\tilde{b}_i}\Big)\Big)\Big]
\end{aligned}
$$

Box contributions

$$
\mathcal{M}_{\sigma\bar{\sigma}\lambda}^{\tilde{q},\Box} = \sum_{i=1}^{6} K_{i\,\sigma\bar{\sigma}\lambda} T_i^{\tilde{q},\Box} \tag{22}
$$

$$
\begin{aligned}
T_1^{\tilde{q},\Box} = \sum_{i,j=1}^{2} \frac{i\, g_S^2}{2\,\pi^2} (& D_{12}^{132,\tilde{b}_i\tilde{b}_i\tilde{t}_j\tilde{t}_j} - D_{12}^{132,\tilde{t}_j\tilde{t}_j\tilde{b}_i\tilde{b}_i} + D_{22}^{132,\tilde{b}_i\tilde{b}_i\tilde{t}_j\tilde{t}_j} - D_{22}^{132,\tilde{t}_j\tilde{t}_j\tilde{b}_i\tilde{b}_i} + D_{24}^{132,\tilde{b}_i\tilde{b}_i\tilde{t}_j\tilde{t}_j} \\
& - D_{24}^{132,\tilde{t}_j\tilde{t}_j\tilde{b}_i\tilde{b}_i} + D_{36}^{132,\tilde{b}_i\tilde{b}_i\tilde{t}_j\tilde{t}_j} - D_{36}^{132,\tilde{t}_j\tilde{t}_j\tilde{b}_i\tilde{b}_i} + D_{23}^{123,\tilde{b}_i\tilde{b}_i\tilde{b}_i\tilde{t}_j} - D_{23}^{123,\tilde{t}_j\tilde{t}_j\tilde{t}_j\tilde{b}_i} + D_{33}^{124,\tilde{b}_i\tilde{b}_i\tilde{b}_i\tilde{t}_j} \\
& - D_{33}^{124,\tilde{t}_j\tilde{t}_j\tilde{t}_j\tilde{b}_i} + D_{37}^{123,\tilde{b}_i\tilde{b}_i\tilde{b}_i\tilde{t}_j} - D_{37}^{123,\tilde{t}_j\tilde{t}_j\tilde{t}_j\tilde{b}_i} - D_{37}^{124,\tilde{b}_i\tilde{b}_i\tilde{b}_i\tilde{t}_j} + D_{37}^{124,\tilde{t}_j\tilde{t}_j\tilde{t}_j\tilde{b}_i})\, g[\tilde{t}_j\tilde{b}_i W^{\pm}]\, g[H^{\pm}\tilde{t}_j\tilde{b}_i]
\end{aligned}
$$

$$
\begin{aligned}
T_2^{\tilde{q},\Box} = \sum_{i,j=1}^{2} \frac{i\, g_S^2}{2\,\pi^2} (& D_{26}^{132,\tilde{b}_i\tilde{b}_i\tilde{t}_j\tilde{t}_j} - D_{26}^{132,\tilde{t}_j\tilde{t}_j\tilde{b}_i\tilde{b}_i} + D_{38}^{132,\tilde{b}_i\tilde{b}_i\tilde{t}_j\tilde{t}_j} - D_{38}^{132,\tilde{t}_j\tilde{t}_j\tilde{b}_i\tilde{b}_i} + D_{23}^{123,\tilde{b}_i\tilde{b}_i\tilde{b}_i\tilde{t}_j} \\
& - D_{23}^{123,\tilde{t}_j\tilde{t}_j\tilde{t}_j\tilde{b}_i} + D_{33}^{124,\tilde{b}_i\tilde{b}_i\tilde{b}_i\tilde{t}_j} - D_{33}^{124,\tilde{t}_j\tilde{t}_j\tilde{t}_j\tilde{b}_i} + D_{39}^{123,\tilde{b}_i\tilde{b}_i\tilde{b}_i\tilde{t}_j} - D_{39}^{123,\tilde{t}_j\tilde{t}_j\tilde{t}_j\tilde{b}_i} \\
& - D_{39}^{124,\tilde{b}_i\tilde{b}_i\tilde{b}_i\tilde{t}_j} + D_{39}^{124,\tilde{t}_j\tilde{t}_j\tilde{t}_j\tilde{b}_i})\, g[\tilde{t}_j\tilde{b}_i W^{\pm}]\, g[H^{\pm}\tilde{t}_j\tilde{b}_i]
\end{aligned}
$$

$$
\begin{aligned}
T_3^{\tilde{q},\Box} = \sum_{i,j=1}^{2} -\frac{i\, g_S^2}{4\,\pi^2} (& -2\, D_{27}^{132,\tilde{b}_i\tilde{b}_i\tilde{t}_j\tilde{t}_j} + 2\, D_{27}^{132,\tilde{t}_j\tilde{t}_j\tilde{b}_i\tilde{b}_i} - 2\, D_{311}^{132,\tilde{b}_i\tilde{b}_i\tilde{t}_j\tilde{t}_j} + 2\, D_{311}^{132,\tilde{t}_j\tilde{t}_j\tilde{b}_i\tilde{b}_i} + C_0^{34,\tilde{b}_i\tilde{t}_j\tilde{b}_i} \\
& - C_0^{34,\tilde{t}_j\tilde{b}_i\tilde{t}_j} + C_{11}^{(12)3,\tilde{b}_i\tilde{b}_i\tilde{t}_j} - C_{11}^{(12)3,\tilde{t}_j\tilde{t}_j\tilde{b}_i} - 2\, D_{27}^{123,\tilde{b}_i\tilde{b}_i d_j\tilde{t}_j} + 2\, D_{27}^{123,\tilde{t}_j\tilde{t}_j\tilde{t}_j\tilde{b}_i} - 2\, D_{311}^{123,\tilde{b}_i\tilde{b}_i\tilde{b}_i\tilde{t}_j} \\
& + 2\, D_{311}^{123,\tilde{t}_j\tilde{t}_j\tilde{t}_j\tilde{b}_i} + 2\, D_{311}^{124,\tilde{b}_i\tilde{b}_i\tilde{b}_i\tilde{t}_j} - 2\, D_{311}^{124,\tilde{t}_j\tilde{t}_j\tilde{t}_j\tilde{b}_i} - 2\, D_{313}^{124,\tilde{b}_i\tilde{b}_i\tilde{b}_i\tilde{t}_j} + 2\, D_{313}^{124,\tilde{t}_j\tilde{t}_j\tilde{t}_j\tilde{b}_i}) \\
& g[\tilde{t}_j\tilde{b}_i W^{\pm}]\, g[H^{\pm}\tilde{t}_j\tilde{b}_i]
\end{aligned}
$$

$$
\begin{aligned}
T_4^{\tilde{q},\Box} = \sum_{i,j=1}^{2} -\frac{i\, g_S^2}{4\,\pi^2} (& -2\, D_{313}^{132,\tilde{b}_i\tilde{b}_i\tilde{t}_j\tilde{t}_j} + 2\, D_{313}^{132,\tilde{t}_j\tilde{t}_j\tilde{b}_i\tilde{b}_i} + C_0^{34,\tilde{b}_i\tilde{t}_j\tilde{b}_i} - C_0^{34,\tilde{t}_j\tilde{b}_i\tilde{t}_j} + C_{11}^{(12)3,\tilde{b}_i\tilde{b}_i\tilde{t}_j} \\
& - C_{11}^{(12)3,\tilde{t}_j\tilde{t}_j\tilde{b}_i} - 2\, D_{27}^{123,\tilde{b}_i\tilde{b}_i\tilde{b}_i\tilde{t}_j} + 2\, D_{27}^{123,\tilde{t}_j\tilde{t}_j\tilde{t}_j\tilde{b}_i} - 2\, D_{312}^{123,\tilde{b}_i\tilde{b}_i\tilde{b}_i\tilde{t}_j} + 2\, D_{312}^{123,\tilde{t}_j\tilde{t}_j\tilde{t}_j\tilde{b}_i} \\
& + 2\, D_{312}^{124,\tilde{b}_i\tilde{b}_i\tilde{b}_i\tilde{t}_j} - 2\, D_{312}^{124,\tilde{t}_j\tilde{t}_j\tilde{t}_j\tilde{b}_i} - 2\, D_{313}^{124,\tilde{b}_i\tilde{b}_i\tilde{b}_i\tilde{t}_j} + 2\, D_{313}^{124,\tilde{t}_j\tilde{t}_j\tilde{t}_j\tilde{b}_i})\, g[\tilde{t}_j\tilde{b}_i W^{\pm}]\, g[H^{\pm}\tilde{t}_j\tilde{b}_i]
\end{aligned}
$$

$$
\begin{aligned}
T_5^{\tilde{q},\Box} = \sum_{i,j=1}^{2} \frac{i\, g_S^2}{4\,\pi^2} (& C_0^{24,\tilde{b}_i\tilde{b}_i\tilde{t}_j} - C_0^{24,\tilde{t}_j\tilde{t}_j\tilde{b}_i} - C_{11}^{(13)2,\tilde{b}_i\tilde{t}_j\tilde{t}_j} + C_{11}^{(13)2,\tilde{t}_j\tilde{b}_i\tilde{b}_i} + 2\, D_{27}^{132,\tilde{b}_i\tilde{b}_i\tilde{t}_j\tilde{t}_j} \\
& - 2\, D_{27}^{132,\tilde{t}_j\tilde{t}_j\tilde{b}_i\tilde{b}_i} + 2\, D_{312}^{132,\tilde{b}_i\tilde{b}_i\tilde{t}_j\tilde{t}_j} - 2\, D_{312}^{132,\tilde{t}_j\tilde{t}_j\tilde{b}_i\tilde{b}_i} + 2\, D_{313}^{123,\tilde{b}_i\tilde{b}_i\tilde{b}_i\tilde{t}_j} - 2\, D_{313}^{123,\tilde{t}_j\tilde{t}_j\tilde{t}_j\tilde{b}_i} \\
& + 2\, D_{313}^{124,\tilde{b}_i\tilde{b}_i\tilde{b}_i\tilde{t}_j} - 2\, D_{313}^{124,\tilde{t}_j\tilde{t}_j\tilde{t}_j\tilde{b}_i})\, g[\tilde{t}_j\tilde{b}_i W^{\pm}]\, g[H^{\pm}\tilde{t}_j\tilde{b}_i]
\end{aligned}
$$

$$
\begin{aligned}
T_6^{\tilde{q},\Box} = \sum_{i,j=1}^{2} \frac{i\, g_S^2}{4\,\pi^2} (& 2\, D_{312}^{132,\tilde{b}_i\tilde{b}_i\tilde{t}_j\tilde{t}_j} - 2\, D_{312}^{132,\tilde{t}_j\tilde{t}_j\tilde{b}_i\tilde{b}_i} - C_{12}^{1(23),\tilde{b}_i\tilde{b}_i\tilde{t}_j} + C_{12}^{1(23),\tilde{t}_j\tilde{t}_j\tilde{b}_i} + 2\, D_{313}^{123,\tilde{b}_i\tilde{b}_i\tilde{b}_i\tilde{t}_j} \\
& - 2\, D_{313}^{123,\tilde{t}_j\tilde{t}_j\tilde{t}_j\tilde{b}_i} + 2\, D_{313}^{124,\tilde{b}_i\tilde{b}_i\tilde{b}_i\tilde{t}_j} - 2\, D_{313}^{124,\tilde{t}_j\tilde{t}_j\tilde{t}_j\tilde{b}_i})\, g[\tilde{t}_j\tilde{b}_i W^{\pm}]\, g[H^{\pm}\tilde{t}_j\tilde{b}_i]
\end{aligned}
$$

B.3 Helicity factors

The factors $K_{i\,\sigma\bar{\sigma}\lambda}$ contain all the helicity information of the amplitude. They are obtained by contracting kinematical Tensors with the helicity four-vectors defined in chapter 2.1. In the following these factors are listed. The symbol λ_T denotes a transverse polarization of the W boson, i.e. $\lambda_T = \pm 1$).

$$K_{1,\sigma\bar\sigma 0} = K_{2,\sigma\bar\sigma 0} = \frac{\left(4\,\hat s\,|\vec p_W|^2 \,-(\,\hat t-\hat u\,)^2\right)\left(2\,|\vec p_W|^2\,\sqrt{\hat s}+E_W\,(\hat u-\hat t)\right)}{32\,(\,\hat s\,|\vec p_W|\,m_W\,)}\,,$$

$$K_{3,\sigma\bar\sigma 0} = \frac{1}{8\,m_W}\left(-\,2\,|\vec p_W|\,\sqrt{\hat s}+\frac{E_W\,(\,\hat t-\hat u\,)}{|\vec p_W|}\right)\,(\sigma\,\bar\sigma+1)\,,$$

$$K_{4,\sigma\bar\sigma 0} = K_{3,\sigma\bar\sigma 0}(\hat t\leftrightarrow\hat u)\,,$$

$$K_{5,\sigma\bar\sigma 0} = K_{6,\sigma\bar\sigma 0} = \frac{E_W}{m_W}\left(\frac{1}{8}\,\frac{(\,\hat t-\hat u\,)^2}{\hat s\,|\vec p_W|}-\frac{1}{2}\,|\vec p_W|\right)\,,$$

$$K_{7,\sigma\bar\sigma 0} = -i\,(\hat s/2)\,\sigma\,K_{5,\sigma\bar\sigma 0}\,,$$

$$K_{8,\sigma\bar\sigma 0} = i\,(\hat s/2)\,\bar\sigma\,K_{5,\sigma\bar\sigma 0}\,,$$

$$K_{9,\sigma\bar\sigma 0} = 0\,,$$

$$K_{10,\sigma\bar\sigma 0} = \frac{i}{16\,m_W}\left(\frac{E_W\,(\,\hat t-\hat u\,)}{|\vec p_W|}-2\,\sqrt{\hat s}\,|\vec p_W|\right)\,\hat s\,(\sigma+\bar\sigma)\,,$$

$$K_{11,\sigma\bar\sigma 0} = K_{10,\sigma\bar\sigma 0}(\hat t\leftrightarrow\hat u)\,,$$

$$K_{12,\sigma\bar\sigma 0} = K_{13,\sigma\bar\sigma 0} = -K_{8,\sigma\bar\sigma 0}\,,$$

$$K_{14,\sigma\bar\sigma 0} = \frac{i\,\left(2\,|\vec p_W|^2\,\sqrt{\hat s}-E_W(\hat t-\hat u)\right)\left(2\,\sqrt{\hat s}\,E_W-\hat t+\hat u\right)}{32\,|\vec p_W|\,m_W}\,(\sigma+\bar\sigma)\,,$$

$$K_{15,\sigma\bar\sigma 0} = \frac{i\,\left(2\,|\vec p_W|^2\,\sqrt{\hat s}+E_W(\hat t-\hat u)\right)\left(2\,\sqrt{\hat s}\,E_W-\hat t+\hat u\right)}{32\,|\vec p_W|\,m_W}\,(\sigma+\bar\sigma)\,,$$

$$K_{16,\sigma\bar\sigma 0} = K_{7,\sigma\bar\sigma 0}\,m_W^2/(E_W\sqrt{\hat s})\,,\qquad K_{17,\sigma\bar\sigma 0} = K_{8,\sigma\bar\sigma 0}\,m_W^2/(E_W\sqrt{\hat s})\,,$$

$$K_{18,\sigma\bar\sigma 0} = (2/\hat s)\,K_{10,\sigma\bar\sigma 0}\,,\qquad K_{19,\sigma\bar\sigma 0} = -K_{15,\sigma\bar\sigma 0}(\hat t\leftrightarrow\hat u)\,,$$

$$K_{20,\sigma\bar\sigma 0} = -K_{14,\sigma\bar\sigma 0}(\hat t\leftrightarrow\hat u)\,,\qquad K_{21,\sigma\bar\sigma 0} = -K_{16,\sigma\bar\sigma 0}\,,$$

$$K_{22,\sigma\bar\sigma 0} = -K_{17,\sigma\bar\sigma 0}\,,\qquad K_{23,\sigma\bar\sigma 0} = -K_{18,\sigma\bar\sigma 0}(\hat t\leftrightarrow\hat u)\,,$$

$$K_{24,\sigma\bar\sigma 0} = -\frac{i\,m_W\,(\,\hat t-\hat u\,)}{4\,|\vec p_W|\,\sqrt{\hat s}}\,(\sigma+\bar\sigma)\,.$$

In the following an additional shorthand is used:

$$p_t^2 = \frac{\hat t\hat u - m_W^2 m_{H^\pm}^2}{\hat s}\,.$$

$$
\begin{aligned}
K_{1,\sigma\bar\sigma\lambda_T} &= -K_{2,\sigma\bar\sigma\lambda_T} = \frac{i}{32}\left(4\sqrt{\hat s}\,|\vec p_W| - \frac{(\hat t-\hat u)^2}{|\vec p_W|\sqrt{\hat s}}\right) p_t\sqrt{2}\,\lambda_T\ ,\\
K_{3,\sigma\bar\sigma\lambda_T} &= -K_{4,\sigma\bar\sigma\lambda_T} = -\frac{i}{8}\frac{\sqrt{2}\,p_t\sqrt{\hat s}\,(\sigma\bar\sigma+1)\,\lambda_T}{|\vec p_W|}\ ,\\
K_{5,\sigma\bar\sigma\lambda_T} &= -\frac{i}{8}\left(\frac{(\hat t-\hat u)\,\lambda_T}{\sqrt{\hat s}\,|\vec p_W|}+2\sigma\right) p_t\sqrt{2}\ ,\\
K_{6,\sigma\bar\sigma\lambda_T} &= K_{5,\sigma\bar\sigma\lambda_T}(\sigma\to-\bar\sigma)\ ,\\
K_{7,\sigma\bar\sigma\lambda_T} &= \frac{1}{2}\left(\frac{1}{4}\,\hat s\,\sigma\,\bar\sigma - \frac{1}{8}\frac{\sqrt{\hat s}\,(\hat t-\hat u)\,\sigma\,\lambda_T}{|\vec p_W|}\right) p_t\sqrt{2}\ ,\\
K_{8,\sigma\bar\sigma\lambda_T} &= K_{7,\sigma\bar\sigma\lambda_T}(\sigma\to-\bar\sigma,\,\bar\sigma\to-\sigma)\ ,\\
K_{9,\sigma\bar\sigma\lambda_T} &= \frac{1}{8}\sqrt{2}\,\hat s\,p_t\,(\sigma\bar\sigma+1)\ ,\\
K_{10,\sigma\bar\sigma\lambda_T} &= -K_{11,\sigma\bar\sigma\lambda_T} = i\,(\hat s/2)\,K_{3,\sigma\bar\sigma\lambda_T}\ ,\\
K_{12,\sigma\bar\sigma\lambda_T} &= i\,(\hat s/2)\,\sigma\,K_{5,\sigma\bar\sigma\lambda_T}\ ,\\
K_{13,\sigma\bar\sigma\lambda_T} &= K_{12,\sigma\bar\sigma\lambda_T}(\sigma\to-\bar\sigma)\ ,
\end{aligned}
$$

$$
\begin{aligned}
K_{14,\sigma\bar\sigma\lambda_T} &= -K_{15,\sigma\bar\sigma\lambda_T} = -\frac{1}{32}\frac{\left(2\sqrt{\hat s}\,E_W-\hat t+\hat u\right)\sqrt{\hat s}\;p_t\sqrt{2}\,(\sigma+\bar\sigma)\,\lambda_T}{|\vec p_W|}\ ,\\
K_{16,\sigma\bar\sigma\lambda_T} &= \frac{1}{16}\left(\left(-\frac{E_W\,(\hat t-\hat u\,)}{|\vec p_W|}+2\,|\vec p_W|\,\sqrt{\hat s}\right)\sigma\,\lambda_T+(\hat t-\hat u)-2\sqrt{\hat s}\,E_W\right) p_t\sqrt{2}\ ,\\
K_{17,\sigma\bar\sigma\lambda_T} &= K_{16,\sigma\bar\sigma\lambda_T}(\sigma\to-\bar\sigma)\ ,\\
K_{18,\sigma\bar\sigma\lambda_T} &= K_{23,\sigma\bar\sigma\lambda_T} = \frac{1}{8}\frac{p_t\sqrt{\hat s}\,\sqrt{2}\,(\sigma+\bar\sigma)\,\lambda_T}{|\vec p_W|}\ ,\\
K_{19,\sigma\bar\sigma\lambda_T} &= -K_{20,\sigma\bar\sigma\lambda_T} = K_{15,\sigma\bar\sigma\lambda_T}(\hat t\leftrightarrow\hat u)\ ,\\
K_{21,\sigma\bar\sigma\lambda_T} &= \frac{1}{16}\left(\left(\frac{E_W\,(\hat t-\hat u\,)}{|\vec p_W|}+2\,|\vec p_W|\,\sqrt{\hat s}\right)\sigma\,\lambda_T+(\hat t-\hat u)+2\sqrt{\hat s}\,E_W\right) p_t\sqrt{2}\ ,\\
K_{22,\sigma\bar\sigma\lambda_T} &= K_{21,\sigma\bar\sigma\lambda_T}(\sigma\to-\bar\sigma)\ ,\\
K_{24,\sigma\bar\sigma\lambda_T} &= -\sqrt{2}\,(E_W/\sqrt{\hat s})\,K_{18,\sigma\bar\sigma\lambda_T}\ .
\end{aligned}
$$

C MSSM couplings

In the following all couplings of the third generation quarks and squarks to MSSM Higgs particles, which are relevant to the process, are collected. The factor $g_2 = e/s_w$ denotes the $SU(2)$ coupling constant of the weak interaction, $s_w = \sin\theta_w$, $c_w = \cos\theta_w$ and $t_w = \tan\theta_w$ with the weak mixing angle θ_w. The scalar and pseudoscalar couplings in the Higgs–fermion interactions are distiguished by adding subscripts 's' and 'p' to the coupling

symbols. Analogously, the subscripts 'v' and 'a' distiguish the vector and axial vector coupling of quarks to the W boson.

C.1 Quark couplings to Higgs bosons

Neutral Higgs bosons

$$g_s[H^0tt] = -g_2\,\frac{m_t}{2m_W}\,\frac{\sin\alpha}{\sin\beta}\,, \qquad g_s[H^0bb] = -g_2\,\frac{m_b}{2m_W}\,\frac{\cos\alpha}{\cos\beta}\,, \tag{23}$$

$$g_s[h^0tt] = -g_2\,\frac{m_t}{2m_W}\,\frac{\cos\alpha}{\sin\beta}\,, \qquad g_s[h^0bb] = +g_2\,\frac{m_b}{2m_W}\,\frac{\sin\alpha}{\cos\beta}\,, \tag{24}$$

$$g_p[H^0tt] = g_p[h^0tt] = 0\,, \qquad g_p[H^0bb] = g_p[h^0bb] = 0\,, \tag{25}$$

$$g_p[A^0tt] = ig_2\,\frac{m_t}{2m_W}\cot\beta\,, \qquad g_p[A^0bb] = ig_2\,\frac{m_b}{2m_W}\tan\beta\,, \tag{26}$$

$$g_s[A^0tt] = g_s[A^0bb] = 0\,. \tag{27}$$

Charged Higgs bosons

$$g_s[H^+\text{ out}, t\text{ in}, b\text{ out}] = g_2\,\frac{m_b\tan\beta + m_t\cot\beta}{2\sqrt{2}m_W} = g_s[H^-\text{ out}, b\text{ in}, t\text{ out}]\,, \tag{28}$$

$$g_p[H^+\text{ out}, t\text{ in}, b\text{ out}] = -g_2\,\frac{m_b\tan\beta - m_t\cot\beta}{2\sqrt{2}m_W} = -g_p[H^-\text{ out}, b\text{ in}, t\text{ out}]\,. \tag{29}$$

C.2 Squark couplings to Higgs bosons

Neutral Higgs bosons

$$g[H^0\tilde{t}_1\tilde{t}_1] = g_2\left[\frac{m_t}{2m_W\sin\beta}\Big((A_t\sin\alpha - \mu\cos\alpha)\sin 2\theta_{\tilde{t}} - 2m_t\sin\alpha\Big)\right.$$
$$\left. + \frac{m_Z\cos(\alpha+\beta)}{6c_w}\Big((5-8c_w^2)\cos^2\theta_{\tilde{t}} - 4s_w^2\Big)\right]\,, \tag{30}$$

$$g[H^0\tilde{t}_2\tilde{t}_2] = g_2\left[\frac{m_t}{2m_W\sin\beta}\Big(-(A_t\sin\alpha - \mu\cos\alpha)\sin 2\theta_{\tilde{t}} - 2m_t\sin\alpha\Big)\right.$$
$$\left. + \frac{m_Z\cos(\alpha+\beta)}{6c_w}\Big(-(5-8c_w^2)\cos^2\theta_{\tilde{t}} + (1-4s_w^2)\Big)\right]\,, \tag{31}$$

$$g[H^0\tilde{b}_1\tilde{b}_1] = g_2\left[\frac{m_b}{2m_W\cos\beta}\Big((A_b\cos\alpha - \mu\sin\alpha)\sin 2\theta_{\tilde{b}} - 2m_b\cos\alpha\Big)\right.$$
$$\left. + \frac{m_Z\cos(\alpha+\beta)}{6c_w}\Big((4c_w^2-1)\cos^2\theta_{\tilde{b}} + 2s_w^2\Big)\right]\,, \tag{32}$$

$$g[H^0\tilde{b}_2\tilde{b}_2] = g_2\left[\frac{m_b}{2m_W\cos\beta}\Big(-(A_b\cos\alpha-\mu\sin\alpha)\sin 2\theta_{\tilde{b}}-2m_b\cos\alpha\Big)\right.$$
$$\left.+\frac{m_Z\cos(\alpha+\beta)}{6c_w}\Big(-(4c_w^2-1)\cos^2\theta_{\tilde{b}}+(1+2c_w^2)\Big)\right], \quad (33)$$

$$g[h^0\tilde{q}_i\tilde{q}_i] = g[H^0,\tilde{q}_i,\tilde{q}_i]\left(\sin\alpha\to\cos\alpha\,,\ \cos\alpha\to-\sin\alpha\right). \quad (34)$$

Charged Higgs bosons

$$g[H^\pm\tilde{t}_1\tilde{b}_1] = \frac{g_2}{2\sqrt{2}m_W}\Big[+2m_tm_b(\tan\beta+\cot\beta)\ \sin\theta_{\tilde{b}}\sin\theta_{\tilde{t}}$$
$$\sin 2\beta\Big(m_b^2(1+\tan^2\beta)+m_t^2(1+\cot^2\beta)-2m_W^2\Big)\ \cos\theta_{\tilde{b}}\cos\theta_{\tilde{t}}$$
$$-2m_b(\mu+A_b\tan\beta)\ \sin\theta_{\tilde{b}}\cos\theta_{\tilde{t}}-2m_t(\mu+A_t\cot\beta)\ \cos\theta_{\tilde{b}}\sin\theta_{\tilde{t}}\Big], \quad (35)$$

$$g[H^\pm\tilde{t}_1\tilde{b}_2] = \frac{g_2}{2\sqrt{2}m_W}\Big[-2m_tm_b(\tan\beta+\cot\beta)\ \cos\theta_{\tilde{b}}\sin\theta_{\tilde{t}}$$
$$+\sin 2\beta\Big(m_b^2(1+\tan^2\beta)+m_t^2(1+\cot^2\beta)-2m_W^2\Big)\ \sin\theta_{\tilde{b}}\cos\theta_{\tilde{t}}$$
$$+2m_b(\mu+A_b\tan\beta)\ \cos\theta_{\tilde{b}}\cos\theta_{\tilde{t}}-2m_t(\mu+A_t\cot\beta)\ \sin\theta_{\tilde{b}}\sin\theta_{\tilde{t}}\Big], \quad (36)$$

$$g[H^\pm\tilde{t}_2\tilde{b}_1] = \frac{g_2}{2\sqrt{2}m_W}\Big[-2m_tm_b(\tan\beta+\cot\beta)\ \sin\theta_{\tilde{b}}\cos\theta_{\tilde{t}}$$
$$+\sin 2\beta\Big(m_b^2(1+\tan^2\beta)+m_t^2(1+\cot^2\beta)-2m_W^2\Big)\ \cos\theta_{\tilde{b}}\sin\theta_{\tilde{t}}$$
$$+2m_b(\mu+A_b\tan\beta)\ \sin\theta_{\tilde{b}}\sin\theta_{\tilde{t}}2m_t(\mu+A_t\cot\beta)\ \cos\theta_{\tilde{b}}\cos\theta_{\tilde{t}}\Big], \quad (37)$$

$$g[H^\pm\tilde{t}_2\tilde{b}_2] = \frac{g_2}{2\sqrt{2}m_W}\Big[2m_tm_b(\tan\beta+\cot\beta)\ \cos\theta_{\tilde{b}}\cos\theta_{\tilde{t}}$$
$$+\sin 2\beta\Big(m_b^2(1+\tan^2\beta)+m_t^2(1+\cot^2\beta)-2m_W^2\Big)\ \sin\theta_{\tilde{b}}\sin\theta_{\tilde{t}}$$
$$+2m_b(\mu+A_b\tan\beta)\ \cos\theta_{\tilde{b}}\sin\theta_{\tilde{t}}+2m_t(\mu+A_t\cot\beta)\ \sin\theta_{\tilde{b}}\cos\theta_{\tilde{t}}\Big]. \quad (38)$$

C.3 Couplings to Gauge bosons

Quarks and Squarks

The indices α, β, a, b are colour indices; i and j denote squark mass-eigenstates.

$$g_v[q^\alpha q^\beta g^a] = g_S \frac{\lambda^a_{\alpha\beta}}{2} \qquad g_a[qqg] = 0 \,, \tag{39}$$

$$g[\tilde{q}^\alpha \tilde{q}^\beta g^a] = -g_S \frac{\lambda^a_{\alpha\beta}}{2} \,, \tag{40}$$

$$g[\tilde{q}^\alpha \tilde{q}^\beta g^a g^b] = g_S^2 \{\frac{\lambda^a}{2}, \frac{\lambda^b}{2}\}_{\alpha\beta} \,, \tag{41}$$

$$g_v[t^\beta b^\alpha W^\pm] = \frac{g_2}{2\sqrt{2}} \delta_{\alpha\beta} \qquad g_a[t^\beta b^\alpha W^\pm] = \frac{g_2}{2\sqrt{2}} \delta_{\alpha\beta} \,, \tag{42}$$

$$g[\tilde{t}_i \tilde{b}_j W^\pm] = -\frac{g_2}{\sqrt{2}} R_{ij} \,, \tag{43}$$

$$g[\tilde{t}_i^\beta \tilde{b}_j^\alpha g^a W^\pm] = \sqrt{2} g_2 g_S R_{ij} \frac{\lambda^a_{\alpha\beta}}{2} \,. \tag{44}$$

The R_{ij} are the following functions of the Squark mixing angles:

$$\begin{pmatrix} R_{11} & R_{12} \\ R_{21} & R_{22} \end{pmatrix} = \begin{pmatrix} \cos\theta_{\tilde{t}} \cos\theta_{\tilde{b}} & \sin\theta_{\tilde{t}} \cos\theta_{\tilde{b}} \\ \cos\theta_{\tilde{t}} \sin\theta_{\tilde{b}} & \sin\theta_{\tilde{t}} \sin\theta_{\tilde{b}} \end{pmatrix} \,. \tag{45}$$

Higgs bosons

$$g[h^0 H^\pm W^\mp] = \frac{g_2}{2} \sin(\beta - \alpha) \,, \tag{46}$$

$$g[H^0 H^\pm W^\mp] = -\frac{g_2}{2} \cos(\beta - \alpha) \,, \tag{47}$$

$$g[A^0 H^\pm W^\mp] = -i \frac{g_2}{2} \,. \tag{48}$$

D Feynman graphs

Feynman Graphs with opposite direction of charge flow are not depicted.

D.1 Quark graphs

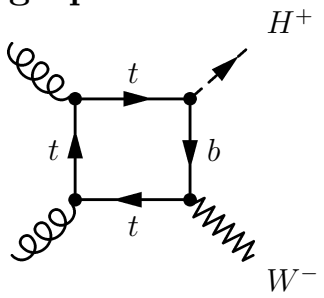

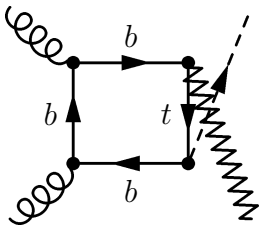

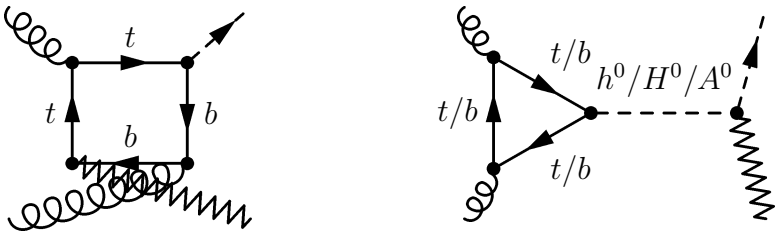

D.2 Squark-Graphs

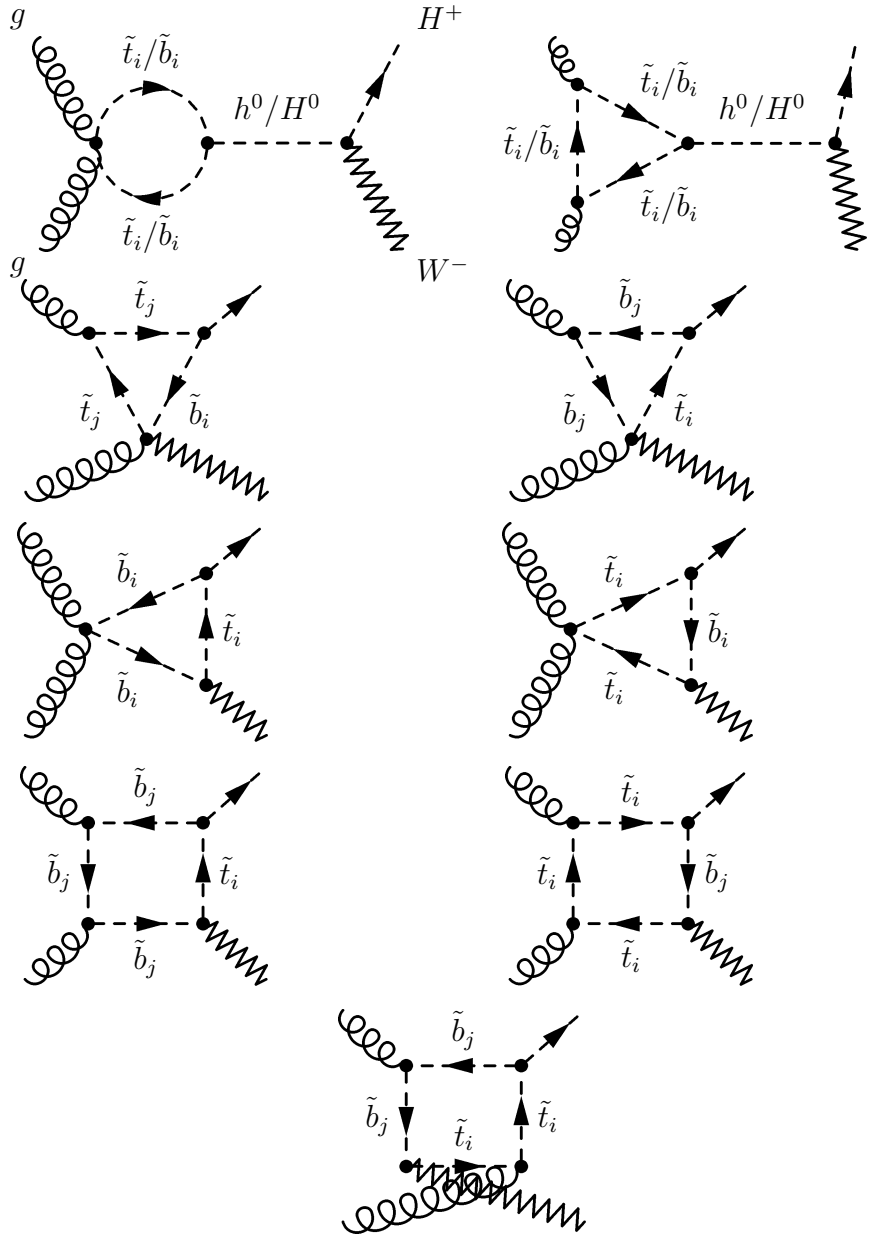

References

[1] ATLAS Collaboration, Technical Design Report, CERN /LHCC/99-15 (1999); CMS Collaboration, Technical Design Reports, CMS-TDR 1–5 (1997,1998).

[2] J.F. Gunion, H.E. Haber, F.E. Paige, W.-K. Tung and S.S.D. Willenbrock, Nucl. Phys. **B294** 621 (1987).

[3] S. Morreti and K. Odagiri, Phys. Rev. **D55** 5627 (1997).

[4] E. Eichten, I. Hinchliffe, K. Lane and C. Quigg, Rev. Mod. Phys. **56** (1984) 579.

[5] A. Krause, T. Plehn, M. Spira and P. M. Zerwas, Nucl. Phys. **B519** (1998) 85;

[6] A. A. Barrientos Bendezu and B. A. Kniehl, Nucl. Phys. **B568** (2000) 305.

[7] O. Brein and W. Hollik, Eur. Phys. J. **C13** (2000) 175;

[8] D. A. Dicus, J. L. Hewett, C. Kao and T. G. Rizzo, Phys. Rev. **D40** (1989) 787.

[9] A. A. Barrientos Bendezu and B. A. Kniehl, Phys. Rev. **D59** (1999) 015009, *ibid* **D61** 097701 (2000).

[10] S. Moretti and K. Odagiri, Phys. Rev. **D59** (1999) 055008 [hep-ph/9809244].

[11] F. I. Olness and W. Tung, Nucl. Phys. **B308** (1988) 813.

[12] Y. S. Yang, C. S. Li, L. G. Jin and S. H. Zhu, hep-ph/0004248.

[13] D. E. Groom *et al.* [Particle Data Group], Eur. Phys. J. **C15** (2000) 1.

[14] G. Cho and K. Hagiwara, Nucl. Phys. **B574** (2000) 623 [hep-ph/9912260].

[15] A. A. Barrientos Bendezu and B. A. Kniehl, hep-ph/0007336.

[16] J. Küblbeck, M. Böhm and A. Denner, Comput. Phys. Commun. **60** (1990) 165; T. Hahn, hep-ph/9905354.

[17] S. Alam, K. Hagiwara, S. Kanemura, R. Szalapski and Y. Umeda, Phys. Rev. D to appear, [hep-ph/0002066].

[18] R. Brock *et al.* [CTEQ Collaboration], *Handbook of perturbative QCD: Version 1.0*, Rev. Mod. Phys. **67** (1995) 157.

[19] A. D. Martin, W. J. Stirling and R. G. Roberts, Phys. Lett. **B354** (1995) 155.

[20] G. Passarino and M. Veltman, Nucl. Phys. **B160** (1979) 151.

[21] G.J. van Oldenborgh and J.A.M. Vermaseren, *Comput. Phys. Commun.* **66** (1991) 1, Z. Phys. **C46** 425 (1990).

[22] A. Bartl, W. Majerotto, B. Mosslacher and N. Oshimo, Z. Phys. **C52** (1991) 477; A. Bartl, W. Majerotto and W. Porod, Z. Phys. **C64** (1994) 499; A. Djouadi, W. Hollik and C. Jünger, Phys. Rev. D **55** (1997) 6975.

Figure Captions

Figure 1 Partonic cross section evaluated using all Feynman graphs (solid lines), only quark loop graphs (dashed lines) and only squark loop graphs (dotted lines) for a sequence of charged-Higgs masses $(100, 210, 360, 450\,\mathrm{GeV})$ and $\tan\beta = 1.5$. The parameter set 1 (see table 2) is used in the squark sector.

Figure 2 Hadronic cross section for H^+W^- production via gluon fusion versus the charged-Higgs mass $m_{H^\pm}$ for two values of $\tan\beta$ (1.5,6). The three squark scenarios without mixing (A, B, C in Table 1) are compared with the case of decoupling squarks (solid lines).

Figure 3 Hadronic cross section for H^+W^- production via gluon fusion versus $\tan\beta$ for three values of the charged-Higgs mass $m_{H^\pm}$ (100,300,1000 GeV). The three squark cases without mixing (A, B, C in Table 1) are compared with the case of decoupling squarks (solid lines).

Figure 4 Hadronic cross section for H^+W^- production via gluon fusion versus the charged-Higgs mass $m_{H^\pm}$ for two values of $\tan\beta$ (1.5,6). The three squark scenarios with large mixing (1, 2, 3 in Table 2) are compared with the case of decoupling squarks (solid lines).

Figure 5 Hadronic cross section for H^+W^- production via gluon fusion versus $\tan\beta$ for three values of the charged-Higgs mass $m_{H^\pm}$ (100,360,1000 GeV). The squark case 1 (thick lines) is compared to the case of decoupling squarks (thin lines).

Figure 6 Hadronic cross section for H^+W^- production via gluon fusion versus $\tan\beta$ for three values of the charged-Higgs mass $m_{H^\pm}$ (100,410,1000 GeV). The squark case 2 (thick lines) is compared to the case of decoupling squarks (thin lines).

Figure 7 Hadronic cross section for H^+W^- production via gluon fusion versus $\tan\beta$ for three values of the charged-Higgs mass $m_{H^\pm}$ (100,470,1000 GeV). The squark case 3 (thick lines) is compared to the case of decoupling squarks (thin lines).

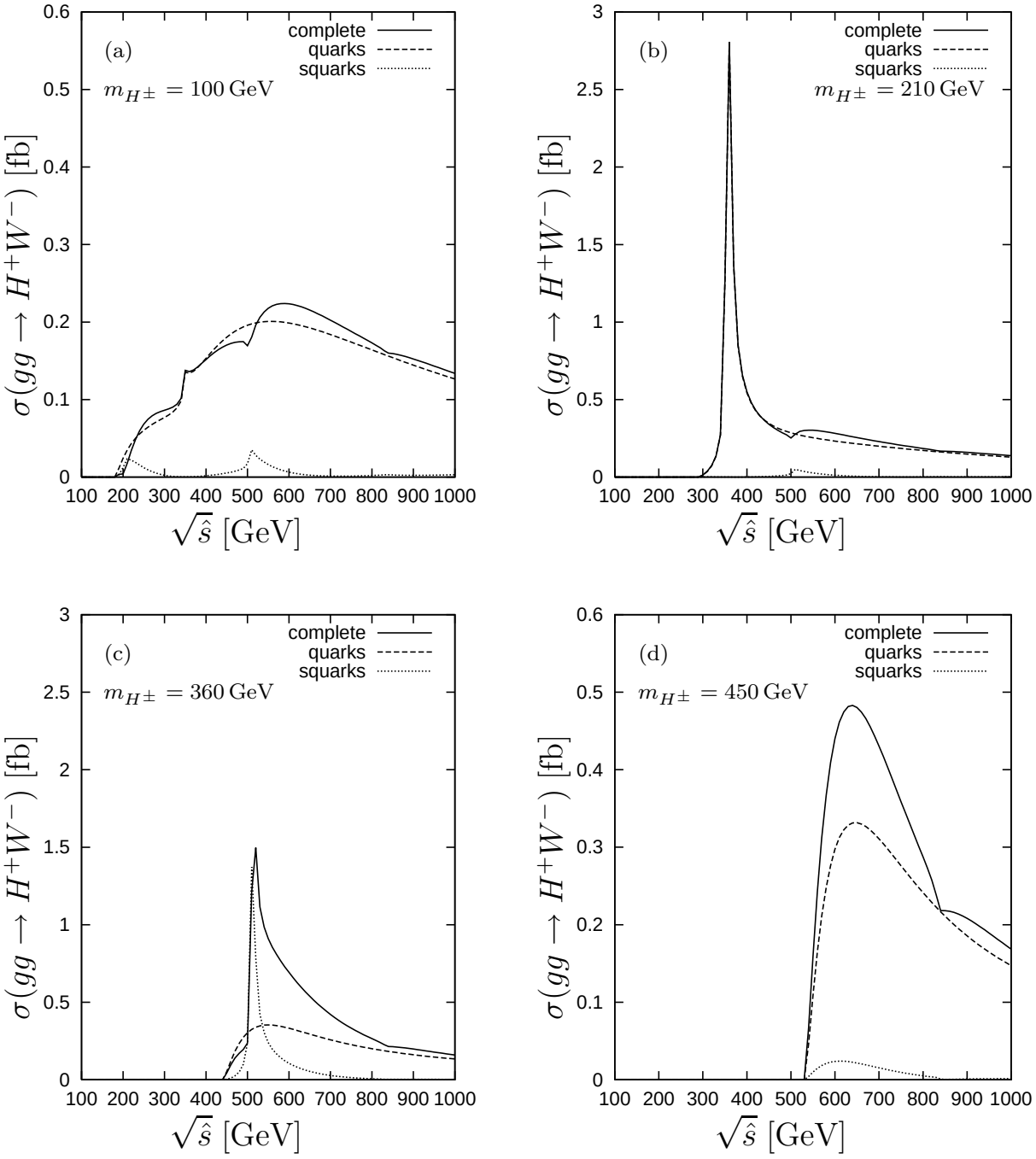

Figure 1: Partonic cross section evaluated using all Feynman graphs (solid lines), only quark loop graphs (dashed lines) and only squark loop graphs (dotted lines) for a sequence of charged-Higgs masses $(100, 210, 360, 450\,\mathrm{GeV})$ and $\tan\beta = 1.5$. The parameter set 1 (see table 2) is used in the squark sector.

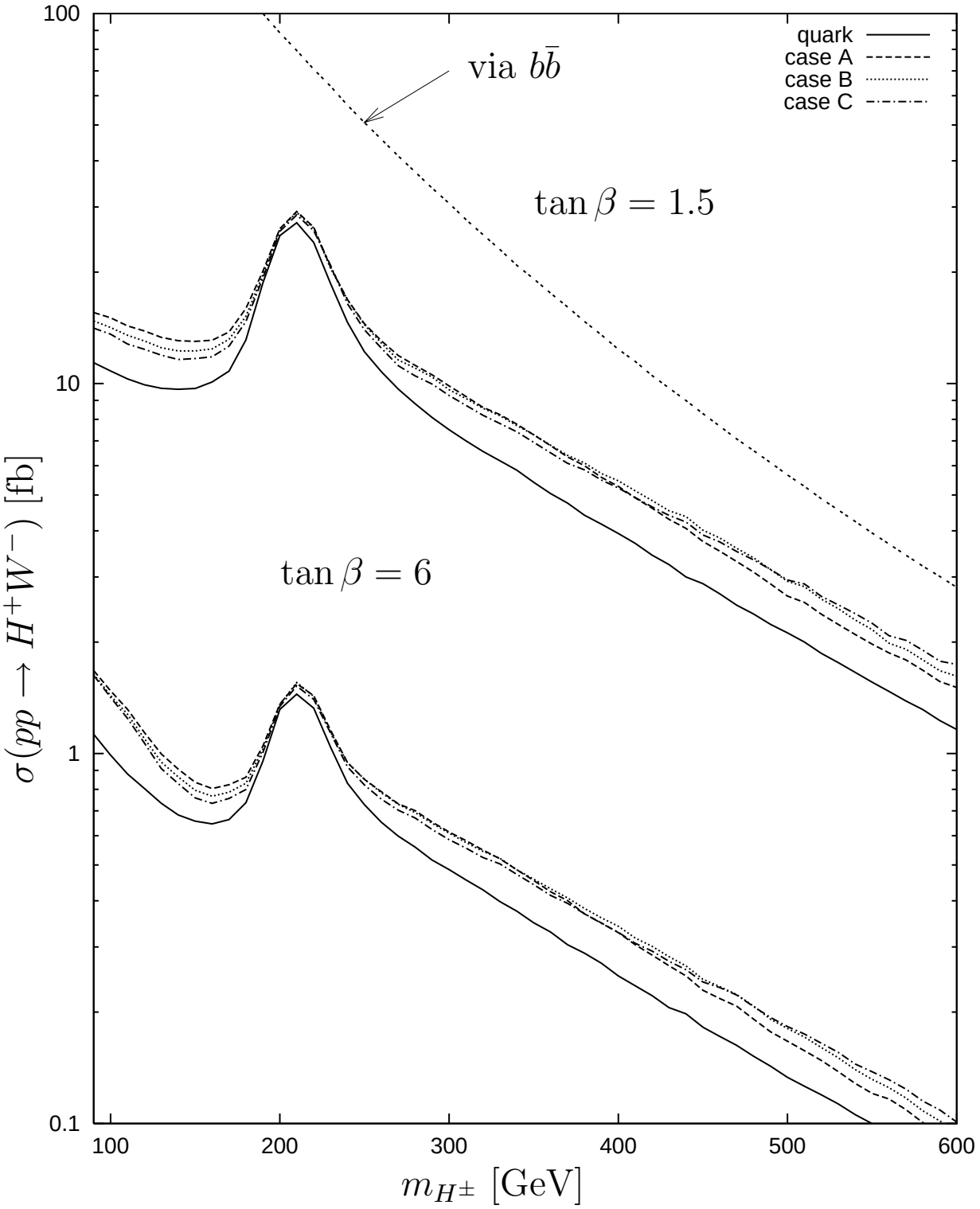

Figure 2: Hadronic cross section for H^+W^- production via gluon fusion versus the charged-Higgs mass $m_{H^\pm}$ for two values of $\tan\beta$ (1.5,6). The three squark scenarios without mixing (A, B, C in Table 1) are compared with the case of decoupling squarks (solid lines).

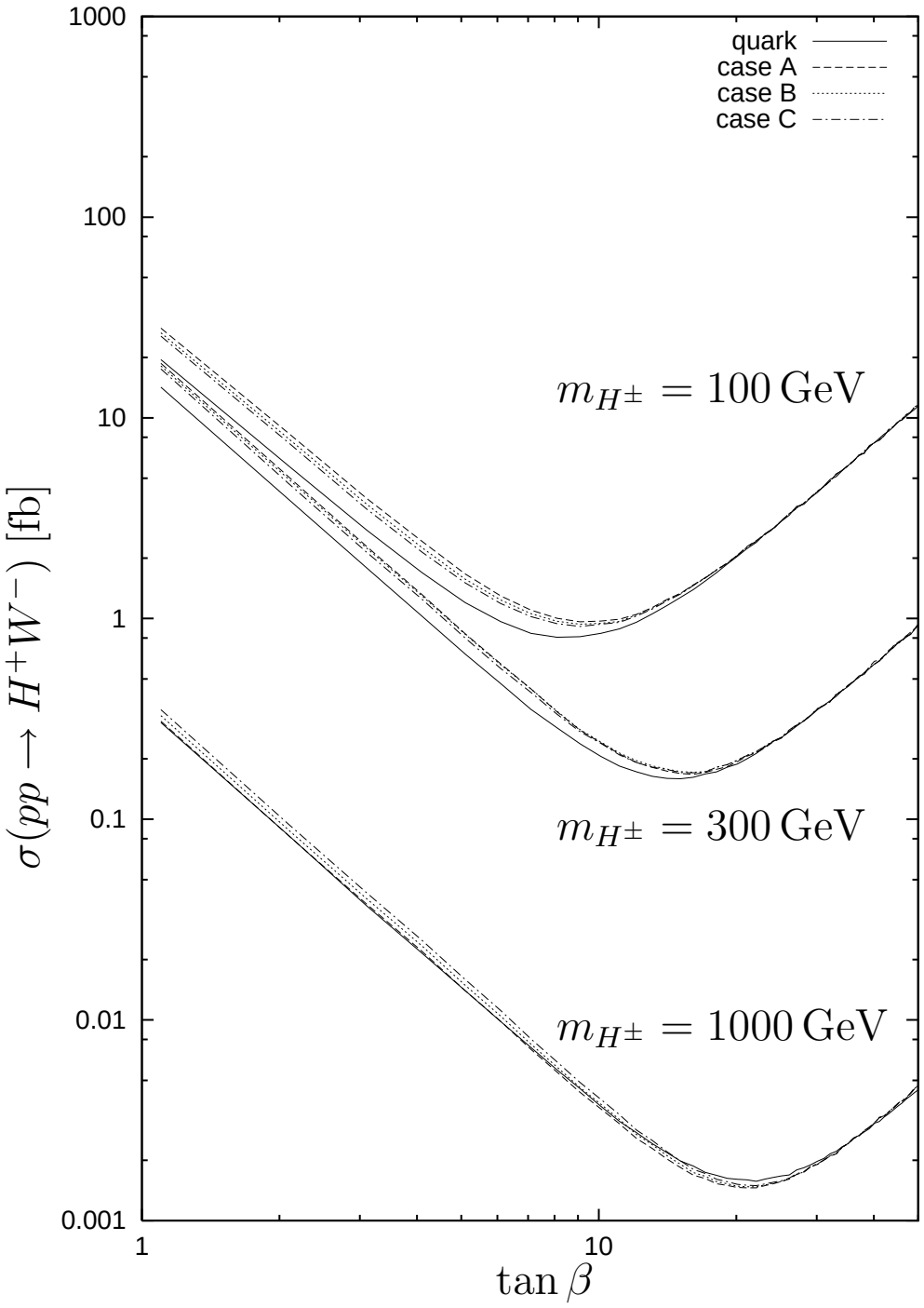

Figure 3: Hadronic cross section for H^+W^- production via gluon fusion versus $\tan\beta$ for three values of the charged-Higgs mass $m_{H^\pm}$ (100,300,1000 GeV). The three squark cases without mixing (A, B, C in Table 1) are compared with the case of decoupling squarks (solid lines).

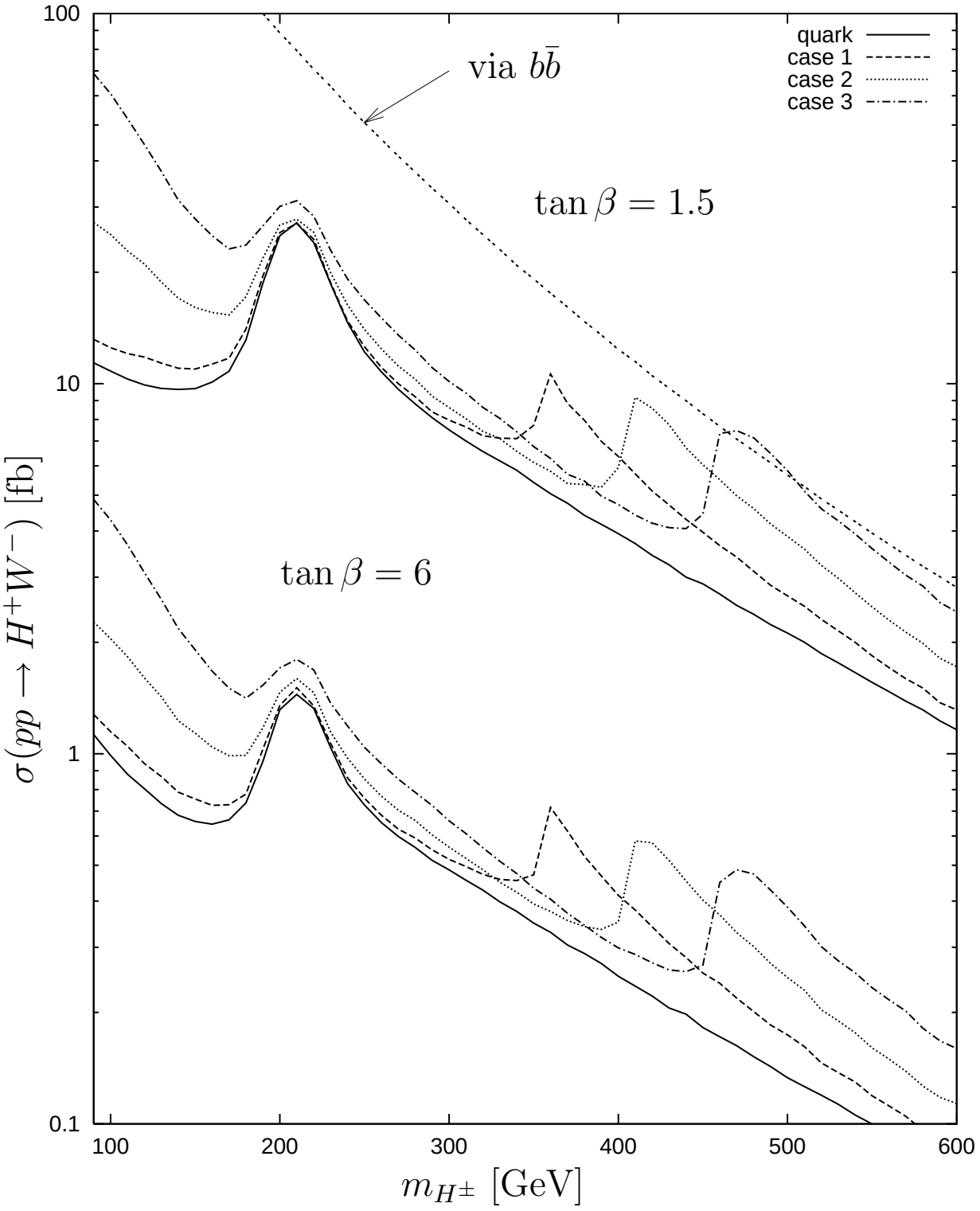

Figure 4: Hadronic cross section for H^+W^- production via gluon fusion versus the charged-Higgs mass $m_{H^\pm}$ for two values of $\tan\beta$ (1.5,6). The three squark scenarios with large mixing (1, 2, 3 in Table 2) are compared with the case of decoupling squarks (solid lines).

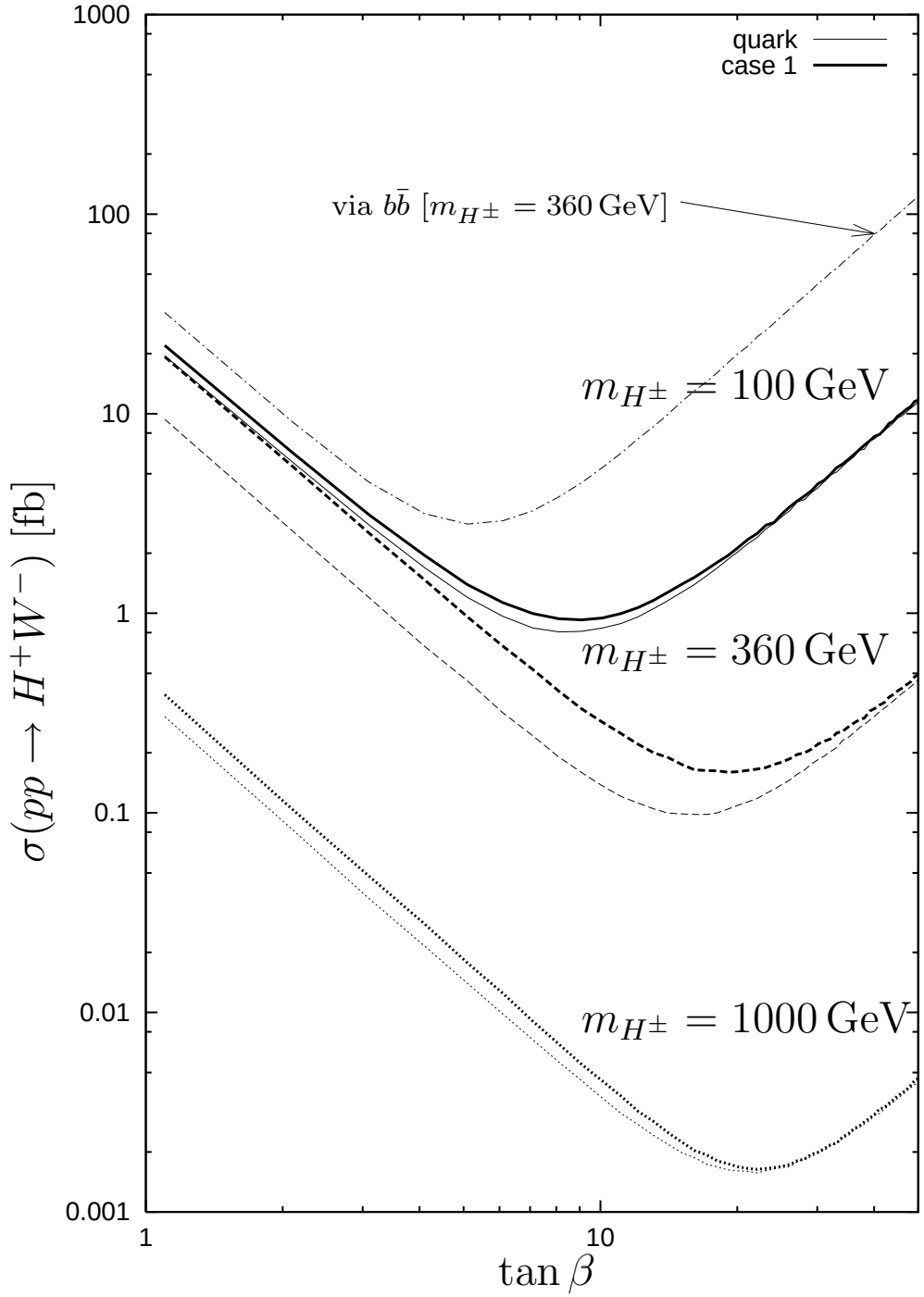

Figure 5: Hadronic cross section for H^+W^- production via gluon fusion versus $\tan\beta$ for three values of the charged-Higgs mass $m_{H^\pm}$ (100,360,1000 GeV). The squark case 1 (thick lines) is compared to the case of decoupling squarks (thin lines).

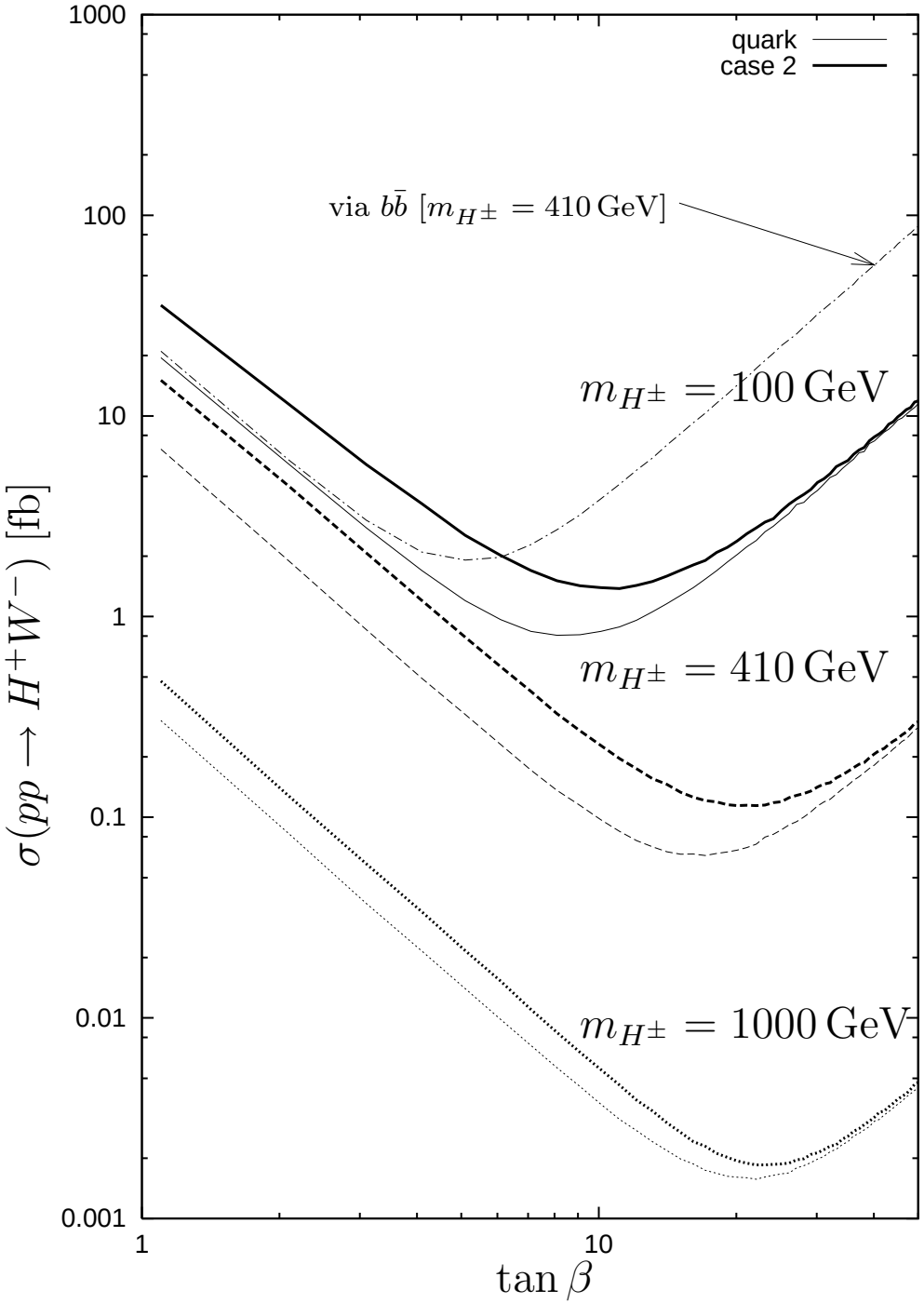

Figure 6: Hadronic cross section for H^+W^- production via gluon fusion versus $\tan\beta$ for three values of the charged-Higgs mass $m_{H^\pm}$ (100,410,1000 GeV). The squark case 2 (thick lines) is compared to the case of decoupling squarks (thin lines).

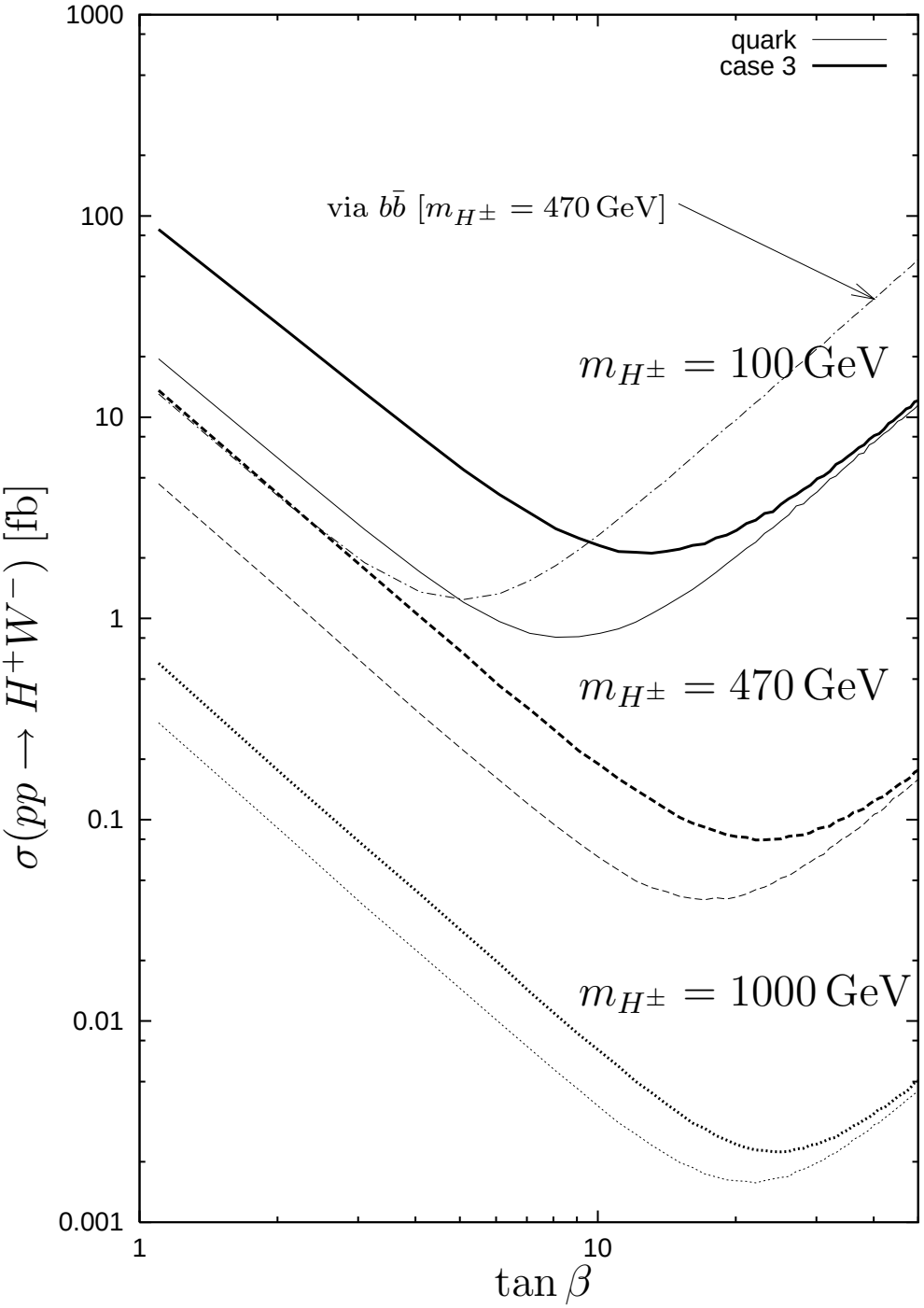

Figure 7: Hadronic cross section for H^+W^- production via gluon fusion versus $\tan\beta$ for three values of the charged-Higgs mass $m_{H^\pm}$ (100,470,1000 GeV). The squark case 3 (thick lines) is compared to the case of decoupling squarks (thin lines).